

New promising bulk thermoelectrics: intermetallics, pnictides and chalcogenides

Antonio P. Gonçalves^{1,a} and Claude Godart²

¹ Campus Tecnológico e Nuclear, Instituto Superior Técnico, Universidade de Lisboa/CFMC-UL, Estrada Nacional 10, 2695-066 Bobadela LRS, Portugal

² Institut de Chimie et des Matériaux de Paris Est (ICMPE), UMR 7182 CNRS, CMTR, 94320 Thiais, France

Received 7 November 2013 / Received in final form 16 December 2013

Published online 19 February 2014 – © EDP Sciences, Società Italiana di Fisica, Springer-Verlag 2014

Abstract. The need of alternative “green” energy sources has recently renewed the interest in thermoelectric (TE) materials, which can directly convert heat to electricity or, conversely, electric current to cooling. The thermoelectric performance of a material can be estimated by the so-called figure of merit, $zT = \sigma\alpha^2T/\lambda$ (α the Seebeck coefficient, $\sigma\alpha^2$ the power factor, σ and λ the electrical and thermal conductivity, respectively), that depends only on the material. In the middle 1990s the “phonon glass and electron crystal” concept was developed, which, together with a better understanding of the parameters that affect zT and the use of new synthesis methods and characterization techniques, has led to the discovery of improved bulk thermoelectric materials that start being implemented in applications. During last decades, special focus has been made on skutterudites, clathrates, half-Heusler alloys, $\text{Si}_{1-x}\text{Ge}_x$, Bi_2Te_3 - and PbTe -based materials. However, many other materials, in particular based on intermetallics, pnictides, chalcogenides, oxides, etc. are now emerging as potential advanced bulk thermoelectrics. Herein we discuss the current understanding in this field, with special emphasis on the strategies to reduce the lattice part of the thermal conductivity and maximize the power factor, and review those new potential thermoelectric bulk materials, in particular based on intermetallics, pnictides and chalcogenides. A final chapter, discussing different shaping techniques leading to bulk materials (eventually from nanostructured TE materials), is also included.

1 Introduction

The increase of energy system’s efficiency and the discovery of new sources of clean energy have become major issues in today’s society, especially after the Kyoto protocol. In fact, the majority of the energy actually produced by man is lost, mainly as waste heat. Just to mention two examples, in a vehicle only $\sim 10\%$ of the energy produced in the internal combustion engine is converted to useful work [1] and 30% of the primary energy generated in the European Union is lost, mostly as heat (EER 2008¹). Thermoelectric (TE) effects allow the direct conversion of heat into electrical energy (Seebeck effect) and, reversibly, use electricity to extract heat (Peltier effect). Therefore, applications include two components: generating electricity from (waste) heat sources and (micro-) cooling. This is why the power generation from waste heat via thermoelectric modules appears these days as one way to improve the global energy efficiency. Besides the aspect of power generation, thermoelectric materials can be used for fine

local cooling, particularly important in the case of removing heat from microelectronic components. However, the low efficiency of TE systems has long limited their interest.

By 1960, most of the TE materials currently used (see Tab. 1) were known and their performance linked to a stagnant zT value of 1, staying undeveloped until 1990 (except in TAGS, compounds of Te-Ag-Ge-Sb , where the role of microstructures seems important). The only main application was based on Bi_2Te_3 for cooling (in suitcase picnic, hotel mini-fridge for the absence of noise, etc.).

A niche application of thermoelectric devices concerned the electricity supply in spacecrafts (like Voyager 1 and 2) with “Radioisotope Thermoelectric Generator”, RTG, in which heat is produced by radioactive decay and used in Si-Ge modules. The lifetime of such systems, favored by the absence of mechanical movements and low maintenance needs, exceeds 30 years.

Either in electricity generation or local cooling, new concepts, including the need to have a good electrical conductivity and poor thermal conduction, lead since 1995 to a quite remarkable progress in thermoelectricity. Two major approaches have been explored together [2]: the search for new solid materials with complex architecture and/or open structure, and the use of nano-structures (quantum

^a e-mail: apg@ctn.ist.utl.pt

¹ Energy and environment report 2008, No 6/2008, European Environment Agency, www.eea.europa.eu.

Table 1. zT of conventional materials in 1960 at their optimum operating temperature T_u ((H)): this value of zT is obtained only in a magnetic field H).

	Bi-Sb	Bi ₂ Te ₃ -Sb ₂ Te ₃	(Bi,Sb) ₂ (Te,Se) ₃	PbTe	Te-Ag-Ge-Sb	Si-Ge
Type	n	n, p	n, p	n	p	n, p
T_u	200	<300	~300–400	...	700	750
zT at T_u	1.1 (H)	0.8	0.9	0.9	1.1	0.6

wells, nanowires, nanograins, thin films, superlattices). These two channels have recently joined in the study of nano-composite solid materials. Among the new materials, many have interesting thermoelectric properties in wider temperature ranges ($-50\text{ }^\circ\text{C} \sim 800\text{ }^\circ\text{C}$), on one hand, and, on the other, higher potential efficiencies. The most studied families of new materials were subject of many reviews in the last decades.

Various groups of oxides were studied: ACoO₃ perovskites [3], AMnO₃ manganites, delafossite CuFeO₂, YBCO (YBa₂Cu₃O_{6+y}), ZnO, ruthenates ARuO₃ A₂RuO₄, In₂O₃, etc. (for a review, see [4,5]). The best zT values reach 0.3–0.4 in p -type and n -type conventional oxides, and 0.56 in oxides with detuned structure (“misfits”), the role of texture on these materials being reviewed [6]. An interesting result concerns In₂O₃: for insertion of Ge exceeding the solubility limit (0.5 at.%), the material forms composite inclusions In₂O₃ + “micron” size (~ 100 microns) of In₂Ge₂O₇, the thermal conductivity is significantly lowered and the $zT = 0.45$ at 1243 K, the best currently observed in n -type oxides [7].

Bi₂Te₃-type telluride compounds and their alloys are actually mainly devoted to Peltier (cooling) applications. These materials were the topic of several reviews, from many years, on bulk [8] or on nanostructured materials [9]. A 50 years review has been given [10] and, more recently, as part of some TE materials or nanocomposites review [11–16].

A review on PbTe has been given [17] and thermoelectric power generation using it has been discussed [18]. New research directions in low dimensional systems [19] and composites have also been reviewed recently [14].

Si-Ge based efficient thermoelectric materials have been discussed for space applications [20] and new directions of research [14,19].

Review of half-Heusler TE materials has been incorporated in more general TE reviews [11,14,21].

Huge literature exists on skutterudites, which have been reviewed time to time from the early years [22–24]. Specific reviews on skutterudites also appear [25,26], these compounds being also discussed as part of a cage like materials review [27].

Clathrates, as new TE materials, have as well been reviewed [21], and their structure, chemical and physical properties discussed [28]. More recent reviews are [11,29].

The role of structures on the thermal conductivity in many TE materials has also been lately discussed [30].

Albeit the large number of review articles dedicated to TE materials in the last decades, main focus has been made on skutterudites, clathrates, half-Heusler alloys, and Si_{1-x}Ge_x-, Bi₂Te₃- and PbTe-based materials. How-

ever, many other materials are now emerging as potential advanced bulk thermoelectrics. Herein we discuss the current understanding in this field, with special emphasis on the strategies to reduce the lattice part of the thermal conductivity and maximize the power factor, and review those new potential thermoelectric bulk materials, in particular based on intermetallics, pnictides and chalcogenides (oxides are not discussed in this review). A final chapter, discussing different shaping techniques leading to bulk materials, is also included.

2 Basic background

The thermoelectric (TE) conversion heat \leftrightarrow electricity appeal to both transport properties in solids, as it is related to the electrical, σ , and thermal, λ , conductivities. In an isotropic and isothermal material the passage of an electric current with a density \vec{j} is associated to an electric field, \vec{E} , by the local Ohm’s law $\vec{E} = \rho\vec{j}$, with ρ the electrical resistivity ($\rho = 1/\sigma = 1/nq\mu_q$), which depends on the carrier concentration, n , and mobility, μ_q , of the charge carriers q (electrons e^- or holes h^+). If a temperature difference is applied to this material in open circuit ($\vec{j} = \vec{0}$), a heat flow, \vec{q} , will flow along the temperature gradient $\vec{\nabla}T$ according to Fourier’s law, $\vec{q} = -\lambda\vec{\nabla}T$, the $-$ sign indicating an opposite direction. Several principal mechanisms contribute to the transport of heat. In metals these are electrons, and the Wiedemann-Franz law relates the “electronic” thermal conductivity, λ_e , to the resistivity, $\lambda_e = LT/\rho$, with L the number of Lorentz

$$L = \frac{\pi^2}{3} \left(\frac{k_B}{e} \right)^2 = 2.45 \times 10^{-8} \text{ V}^2 \text{ K}^{-2}.$$

In insulating materials the heat is mainly transported by the atomic lattice vibrations, or phonons, and thermal conductivity, λ_L , may be given, in a first approximation, by the Debye relationship, $\lambda_L = 1/3 C_p l v$, with C_p the specific heat per unit volume, l the mean free path of the phonons and v the speed of sound. In semiconductors, heat is transported by the two mechanisms and $\lambda = \lambda_e + \lambda_L$. The simultaneous flow of heat and charge in a material leads to the thermoelectric effects.

2.1 The thermoelectric (TE) effects

The first TE effect was discovered by Seebeck [31]: an electrical potential difference, ΔV , appears at the junction of

two materials, a and b, subjected to a temperature difference, ΔT . The Seebeck coefficient of such circuit, α_{ab} , is defined by:

$$\alpha_{ab} = \lim_{\Delta T \rightarrow 0} \Delta V / \Delta T \quad (1)$$

and reflects the formation of an electrical potential gradient in each of the materials when submitted to a thermal gradient. For a particular material, a, and temperature, T , the Seebeck coefficient is given by:

$$\alpha_a(T) = dV_a(T)/dT \quad (2)$$

and we have

$$\alpha_{ab}(T) = \alpha_a(T) - \alpha_b(T) \quad (3)$$

$\alpha_a(T)$ being the measure of the transport entropy, S_a , per charge carrier, q , for such material ($\alpha_a = S_a/q$).

A few years later Peltier [32] discovered the second TE effect: a temperature difference appears at the junction of two materials, a and b, subjected to an electric current, I , with heat release, Q , to a junction and heat absorption in the other junction. The Peltier coefficient $\Pi_{ab}(T)$ is then defined by:

$$\Pi_{ab}(T) = Q/I. \quad (4)$$

Similarly to the Seebeck coefficient, the Peltier coefficient of a junction reflects the presence a Peltier coefficient for each material

$$\Pi_{ab}(T) = \Pi_a(T) - \Pi_b(T). \quad (5)$$

The third TE effect, the Thomson effect [33], is highlighted when a temperature gradient and electric current are simultaneously present: a certain material subjected to a temperature gradient and through which pass an electric current exchange heat with the outside environment. Conversely, an electrical current is generated by a material subjected to a temperature gradient and traversed by a heat flux. Then, in a circuit there is generation or absorption of heat in each individual segment. The flow thermal gradient in the material is given by:

$$dQ/dx = \tau IdT/dx \quad (6)$$

where x is the spatial coordinate and τ is the Thomson coefficient of the material. Thomson (Lord Kelvin) also showed that the Seebeck and Peltier effects are related, $\Pi = \alpha T = Q/I$.

For the refrigeration or generation of electricity by TE effect, a module consists of couples electrically connected (see Fig. 1).

Each couple consists of a p -type material ($\alpha > 0$) and an n -type material ($\alpha < 0$), having a conduction by electrons and holes, respectively. These two materials are joined by a conductive material whose TE power is assumed to be zero. The two branches (p and n) of the couple, and all the other couples realizing the module are connected electrically in series and thermally in parallel.

For cooling, the electric current is applied in such a way that the charge carriers move from the cold source

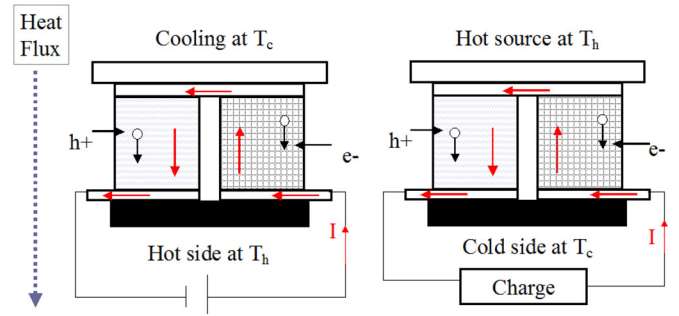


Fig. 1. TE module for electricity generation (right) or cooling (left).

to the hot source in the two branches of the couple. In doing so, they contribute to the transfer entropy from the cold source to the hot spring. For electricity generation, thermal agitation repels charge carriers (n and p) from the hot zone and creates an electrical current.

2.2 Efficiencies, figure of merit

The efficiency of a thermoelectric device depends on many factors, as electrical connections, type of solder, laterals heat losses, etc., which must be optimized in order to maximize it. However, one of the most critical factors are the TE characteristics of the n -type and p -type constituent materials. The performance of a certain material for TE applications is determined by its figure of merit

$$zT = \alpha^2 T \sigma / \lambda = \alpha^2 T / \rho \lambda, \quad (7)$$

where T represents the absolute temperature, α is the Seebeck coefficient, ρ is the electrical resistivity, and σ and λ are the electrical and thermal conductivities, respectively. A good TE material should have high α and σ , and small λ . This is easily understandable: for instance, insulators usually have high α , but their low σ prevents the current flow, making them unsuitable for TE applications; similarly, materials with high λ are also not suitable, as it is difficult to establish the large temperature gradients needed to have high efficiencies (see below). It is interesting to notice that zT depends only on the physical properties of the materials, their TE performance increasing with the increase of the figure of merit.

For a TE cooling system the efficiency is given by its coefficient of performance, COP, which, if optimized, has a maximum value of

$$COP_{\max} = \frac{(1 + ZT)^{1/2} T_c - T_h}{(T_c - T_h) (1 + (1 + ZT)^{1/2})} \quad (8)$$

T_h and T_c being the hot and cold temperatures, respectively, and ZT the figure of merit of the thermoelectric couple, with

$$Z = \frac{(\alpha_p - \alpha_n)^2}{(\sqrt{\lambda_p \rho_p} + \sqrt{\lambda_n \rho_n})^2} \quad (9)$$

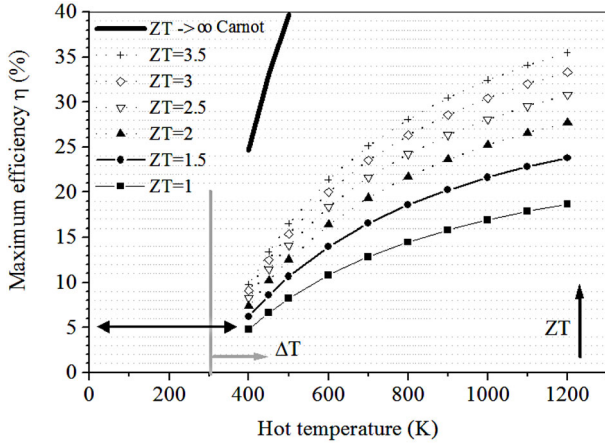


Fig. 2. Theoretical maximum efficiency in electricity generation (cold source assumed at 300 K).

and

$$T = \frac{T_h + T_c}{2} \quad (10)$$

(notice that the figure of merit of the TE couple is represented by ZT , in contrast to the figure of merit of the materials, which is represented by zT). The maximum value of the conversion efficiency for electricity generation can also be determined, being given by:

$$\eta_{\max} = \frac{(T_h - T_c) \left((1 + ZT)^{1/2} - 1 \right)}{T_c + (1 + ZT)^{1/2} T_h}. \quad (11)$$

This expression is used to evaluate the maximum efficiency that can be expected for a TE generator (Fig. 2) depending on the temperature of the heat source (the cold temperature is room temperature, 300 K, indicated by a vertical bar).

The horizontal double arrow shows that for a ZT of 1 and a gradient of 100 °C, the maximum efficiency is 5%. We observe that the efficiency can be increased with the hot temperature (ΔT) for the same ZT and at a given temperature increases with ZT . In both cases, this leads to a problem of materials: to increase their zT and to make materials more stable at high temperatures.

We can see that in both cases (cooling or electricity generation) (i) the Seebeck coefficients of the TE materials must be high and have opposite sign, (ii) their electrical resistivities must be low and (iii) their thermal conductivities must be low. In other words, the figures of merit of both materials must be high in order to maximize the devices coefficient of performance or efficiency. However, this is not easy, as low electrical resistivity is characteristic of metals while high Seebeck coefficients exist on insulators.

Whatever the dimensionality of the system on a basic way, the relative error

$$\frac{\Delta ZT}{ZT} = 2\Delta\alpha/\alpha + \Delta\sigma/\sigma + \Delta\lambda/\lambda (+\Delta T/T)$$

is high (>10%) and announcement effects should be viewed with caution. Generally, we will retain the values

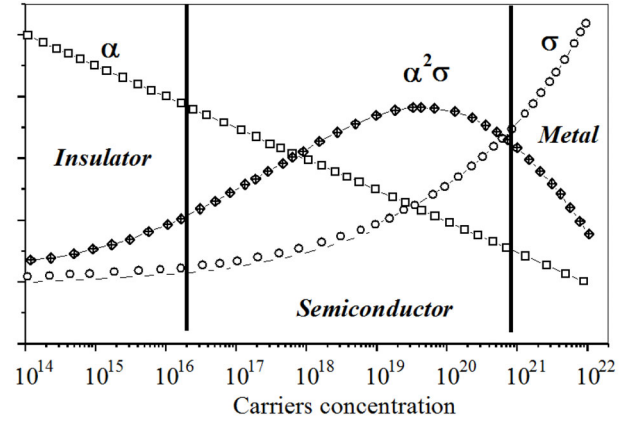


Fig. 3. Influence of the concentration of charge carriers in the thermoelectric power, electrical conductivity and power factor.

quoted by the authors, being aware that values to 2 decimals, or a record between 1.47 and 1.52 for example, are not significant.

2.3 Factors controlling zT : power factor, thermal conductivity, phonon scattering

The previous preliminary calculation assumes that zT is constant with temperature, which is obviously wrong (see its change in the $zT(T)$ curves).

The expression of zT epitomizes the difficulty to optimize the transport properties of a TE material. Indeed, the material must have good electrical conductivity, characteristic of metals, and poor thermal conductivity, characteristic of the insulating materials, simultaneously. The numerator of the figure of merit zT , $\alpha^2\sigma$ is called power factor, PF.

Figure 3 shows the evolution of the thermoelectric power, electrical conductivity and power factor, PF, versus the logarithm of the concentration of charge carriers in the system. The best values of PF are observed in the range of concentration of charge carriers from 10^{18} cm^{-3} to 10^{21} cm^{-3} , i.e. for a semiconductor with low gap (the ideal value of the gap is a few kT [34,35]). Looking for good thermoelectric materials should, according to this model, be limited to degenerate or heavily doped semiconductors. The different approaches adopted to increase the PF were reviewed in reference [2].

The second important factor in the expression of the figure of merit, zT , (in addition to PF) is the thermal conductivity, λ : a material will have optimal TE properties with a low λ . Indeed, high λ tends to oppose the establishment of the thermal gradient.

In a solid λ is mainly composed by two contributions, electronic, λ_e , due to the movement of carriers, and lattice, via the phonons, λ_L , ($\lambda = \lambda_e + \lambda_L$). The electronic part of the thermal conductivity is related to the electronic conductivity via the Wiedemann-Franz law ($\lambda_e = L\sigma T$). By replacing its two components λ_e and λ_L , and applying

the Wiedemann-Franz law, we have:

$$zT = \frac{\alpha^2 T \sigma}{L T \sigma + \lambda_L} \quad \text{either} \quad zT = \frac{\alpha^2}{L} \frac{\lambda_e}{\lambda_e + \lambda_L}.$$

Given this expression, it is clear that the optimization of zT requires the minimization of the phonon contribution to the thermal conductivity. If it is made negligible compared to the electronic contribution, a $zT = 3$ could be obtained for $\alpha = 270 \mu\text{V K}^{-1}$ ($zT = 3$ corresponds to a coefficient of performance refrigeration 1.1, close to that of a compression refrigerator). However, this minimization must not be at the expenses of the electrical conductivity, since the above equation clearly shows that zT increases with λ_e/λ_L and therefore with σ/λ_L . This leads to the proposal of Slack to check for materials that conduct electricity like a crystal and heat like a glass “phonon glass and electron crystal” [36]. It is therefore necessary to find selective diffusion processes having a stronger influence on the propagation of phonons than on the charge carriers.

The physical processes responsible for a large phonon scattering most commonly used in TE bulk materials are many, and include:

- materials with complex crystal structure, thereby increasing the number of optical phonon modes, heat being transmitted primarily by the 3 acoustic modes;
- inclusion of heavy atoms in the cages of the crystalline structure that may vibrate independently of the network (“rattling”) and thus create new phonon modes (very low dispersive optical modes);
- formation of solid solutions between different materials of the same type or existence of vacancies, for which the increase of the disorder induced a significant phonon scattering by a phenomenon of mass fluctuations on one or more crystallographic sites [37]; this may also be obtained by the presence of gaps;
- the phonon scattering by impurities or point defects [38–40], which lead to study the formation of “composite” materials, mixing a good thermoelectric material and another neutral for the point of view of TE, nanocomposites or synthetic techniques (or development of techniques) for “exotic” forms, inducing significant concentrations of point defects.

A final mechanism concerns the importance of scattering by grain boundaries, which leads also to study nanocrystalline materials in order to reduce the mean free path of phonons [41], but also to modify the band structure.

Note that these processes are not exclusive and that many of them can exist simultaneously in the same material. These different mechanisms have been used in the search for new bulk TE materials, and have already lead to significant progresses but currently inconclusive: zT is always up to ~ 2.0 .

2.4 State of the art of bulk TE materials

The use of the different previously described processes to optimize the TE figure of merit (maximize the PF and/or

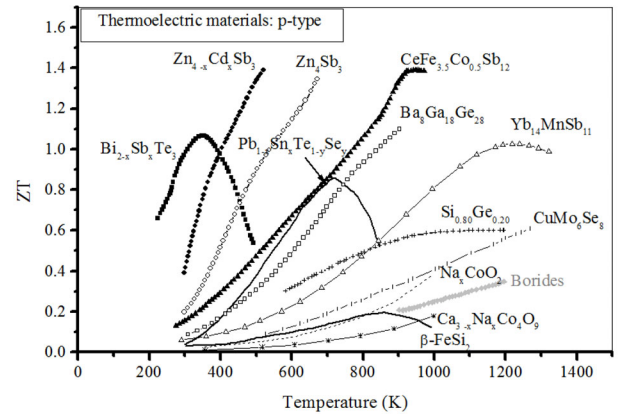


Fig. 4. Larger values of zT for bulk materials (non-exhaustive) p -type (Ref. [43]).

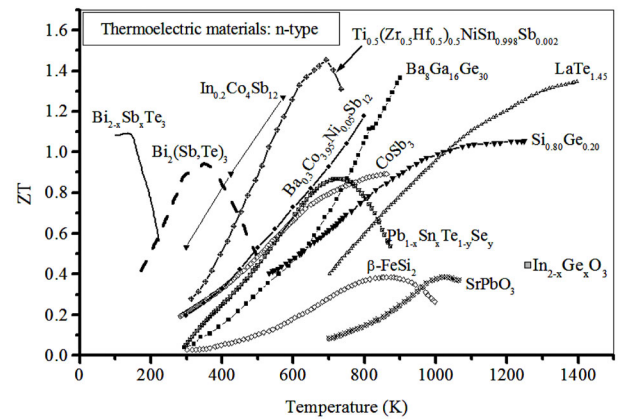


Fig. 5. Larger values of zT for bulk materials (non-exhaustive) n -type (Ref. [43]).

minimize the thermal conductivity) led to a significant increase in zT values. From ~ 1995 several new families of high-performance TE compounds were identified [35,42].

In addition, the discovery of new families also extended the temperature ranges where thermoelectricity can be used. The maximum value of zT in several families reached >1.4 . The best value reported in a bulk material is currently ~ 2 (see tellurides section) [44], but has not been confirmed. The curves of some of the best values of $zT(T)$ currently obtained in bulk materials are shown in Figures 4 and 5 for p - and n -types, respectively. A detailed description of the different families and structures can be found in reference [43] and internal references.

3 New promising bulk thermoelectrics

During the last decades special focus has been made on TE materials like skutterudites, clathrates, half-Heusler alloys, $\text{Si}_{1-x}\text{Ge}_x$ -, Bi_2Te_3 - and PbTe -based. However, many others are now emerging as potential advanced bulk TEs. In particular, those materials based on intermetallics (such as metal silicides, borides, borocarbides and gallides), pnictides (like antimonides and bismuthides), chalcogenides (as tellurides, selenides and sulfides), conducting

organics (such conducting polymers), etc., have recently seen an increasing interest.

Due to their actual and potential importance, individual sections on silicides, antimonides, tellurides, sulfides and selenides are presented below. The other interesting systems are compiled in one part, except those for use at low and cryogenic temperatures, which were separated due to their specificity.

3.1 Silicides

Silicide-based materials were proposed for TE applications already a long time ago [45]. However, a renewed interest in these materials has recently emerged, due to their cheapness, low toxicity, and structural, chemical and thermal stability. Nevertheless, only a few review articles were dedicated to silicides for TE until now [46–48].

The normal requirement to obtain a semiconducting behavior is that all bands should be completely empty or completely filled, in order to have a gap. Many silicon semiconducting compounds that can be used as thermoelectrics have complex structure of conduction or valence band. They usually are Si-rich silicides, except for the case of compounds with alkali and alkaline earth elements. This can be easily understood, as a high concentration of transition metals would result in a metallic behavior (due to the contribution of metal-metal bonds), and alkali and alkaline earth elements have only one and two valence electrons (and, consequently, a higher concentration of these elements is needed to fill the bands).

Mg₂Si-based materials are one of the most studied families of silicides for TE, the good properties arising from the multi-valley character of the conduction band. The effect of doping on Mg₂Si can be very diverse. In Bi-doped Mg₂Si (Mg₂Si:Bi = 1:*x*) fabricated by SPS, the electrical resistivity, Seebeck coefficient, and thermal conductivity are strongly affected by the Bi concentration, the sample of *x* = 0.02 showing a maximum value of *zT* of 0.86 at 862 K [49] or 0.74 at 840 K [50]. 2% Bi doped Mg₂Si with single wall carbon nanohorns (horn-shaped sheath aggregates of graphene sheets) added have a *zT* value of 0.39 at 873 K [51]. Mg₂Si crystals, grown by the vertical Bridgman method and doped with Bi, show a *zT* of 0.65 at 840 K [52]. P-doped Mg₂Si (Mg₂Si:P = 1:*x* (0.0005 ≤ *x* ≤ 0.03)) fabricated by SPS are *n*-type. The resistivity and Seebeck coefficient are strongly affected by *x*, but not the thermal conductivity, and *zT* = 0.33 at 865 K is obtained [53]. With Sb doping, *zT* reaches 0.56 at 862 K, as the thermal conductivity is also affected [54,55], or 0.46 at 810 K [56].

Adding Al to Mg₂Si leads to *n*-type behavior with improved *zT*. On a ball milled and SPS treated (Mg₂Si):Al_{0.01} sample a *zT* = 0.5 at 870 K is observed [57].

Doping with Al, Bi, Sb, La, Li, Ag, In, and Y into Mg₂Si was achieved by a reduction reaction of Mg, Si, and a small amount of metal oxide, carbonate, or hydroxide additive (Al₂O₃, Bi₂O₃, Sb₂O₃, La(OH)₃, Li₂CO₃,

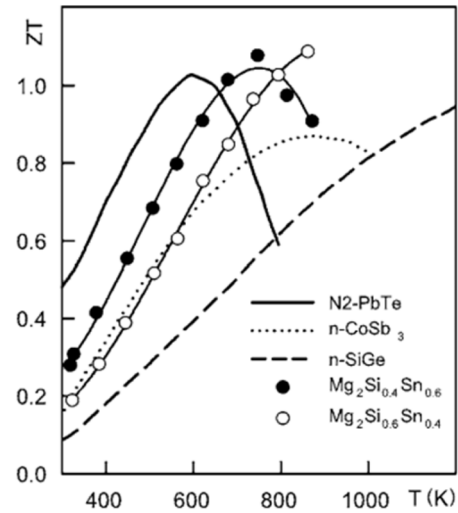


Fig. 6. Higher *zT* of Mg₂Si_{1-x}Sn_x (Ref. [61]).

Ag₂O, CuO, Ga₂O₃, In₂O₃, Na₂CO₃, or Y₂O₃). The maximum values of *zT* for the Mg₂Si composites using Al₂O₃, Bi₂O₃, and Sb₂O₃ were found to be 0.58, 0.68, and 0.63 at ~865 K, respectively [58].

N-type Sc- and Y-doped Mg₂Si prepared by field-activated and pressure-assisted reactive sintering (~SPS) creates an average grain size of ~2 μm (in the Y-doped alloy), which is smaller than that of the sintered pure material. Doping increases the PF and reduces the thermal conductivity, improving *zT* to 0.23 at 600 K [59].

The alloying with Ca in Mg₂Si decreases the PF, *zT* reaching 0.41 and 0.34 at 660 K for Mg₂Si and Mg_{1.99}Ca_{0.01}Si, respectively [60].

The study of Mg₂Si-Mg₂Sn solid solutions was also performed. *zT* values of 0.5 were obtained for Mg₂Si_{0.4}Sn_{0.6} and Mg₂Si_{0.6}Sn_{0.4} due to the relatively low-charge carrier concentrations of the samples [62]. Mg₂Si_{1-x}Sn_x solid solutions prepared by microwave irradiation show a maximum *zT* = 0.26 at 500 K for Mg₂Si_{0.4}Sn_{0.6} [63]. The optimization of electron energy spectrum in the Mg₂Si-Mg₂Sn solid solutions allowed to develop very efficient thermoelectrics with *zT*_{max} ~ 1.1 at 700–800 K when *x* = 0.6 in Mg₂Si_{1-x}Sn_x [61,64] (see Fig. 6). It is interesting to observe that *zT* maximum occurs when the mass difference is maximum, i.e., for *x* ~ 0.5. Moreover, recent calculations point to even higher figures of merit for these solid solutions [65].

Doping of solid solutions was also attempted with the objective to improve the TE performance of Mg₂Si-based materials. *N*-type Al-doped Mg₂Si_{0.9}Sn_{0.1} shows a maximum value of *zT* of 0.68 at 864 K, which is 6 times larger than that of undoped Mg₂Si_{0.9}Sn_{0.1} [66]. Mg₂Si_{0.58}Sn_{0.42-x}Bi_x (0 ≤ *x* ≤ 0.015) are composites of magnesium silicide solution phase and (a minor) magnesium stannide solution phase, with a maximum *zT* = 0.65 at 700 K for *x* = 0.015 [67]. The effect of GaSb addition on the Mg₂Si_{0.5}Sn_{0.5} TE properties has been investigated, and a maximum *zT* = 0.47 was obtained at 660 K for Mg₂Si_{0.5}Sn_{0.5}-0.08GaSb, mainly due to its high

electrical conductivity [68]. The highest figures of merit for n -type materials were recently identified on inhomogeneous $\text{Mg}_2\text{Si}_{0.55}\text{Sn}_{0.4}\text{Ge}_{0.05}$ alloys doped with Bi and Sb, with values of ~ 1.4 and ~ 1.2 at high temperatures for Bi and Sb members, respectively [69].

The TE properties of Mg_2Si -based p -type materials were also improved by doping and/or substitutions, but with much poor results. $\text{Mg}_2\text{Si}:\text{Ga}_x$ and $\text{Mg}_2\text{Si}_{0.6}\text{Ge}_{0.4}:\text{Ga}_x$ alloys exhibit p -type conductivity and a maximum value of $zT \sim 0.36$ was reached for $\text{Mg}_2\text{Si}_{0.6}\text{Ge}_{0.4}:\text{Ga}$ (0.8%) [70]. Similar values were observed in $\text{Mg}_{2(1+z)}(\text{Si}_{0.3}\text{Sn}_{0.7})_{1-y}\text{Ga}_y$ materials [71]. Slightly higher zT values were obtained in $\text{Mg}_2(\text{Ge},\text{Sn})$ compounds doped with Ag ($zT \sim 0.38$ for $\text{Mg}_{1.98}\text{Ge}_{0.4}\text{Sn}_{0.6}\text{Ag}_{0.02}$ at 675 K) [72].

In CoSi, a n -type material, porosity affects the thermal conductivity, the highest value of the figure of merit being obtained in samples prepared from micron-size powder (0.23 at 925 K) [73]. Ge doping in $\text{CoSi}_{0.9}\text{Ge}_{0.1}$ leads to a $zT = 0.11$ at 350 K [74]. Pt is immiscible with CoSi, while Ni and Pd are effective n -type dopants, a $zT = 0.13$ being obtained for $\text{Co}_{0.99}\text{Pt}_{0.01}\text{Si}$ at 300 K [75].

In the orthorhombic compound Ru_2Si_3 , due principally to the larger Seebeck coefficient along the [010] direction, zT is anisotropic (0.2 at 900 K along [010]; zT [010]/ zT [100] > 4 at 900 K), whereas thermal conductivity is not affected by orientations [76].

$\text{MnSi}_{1.7-1.75}$ higher manganese silicides (HMS) concern a series of compounds with general formula $\text{Mn}_n\text{Si}_{2n-m}$ (as Mn_4Si_7 , $\text{Mn}_{11}\text{Si}_{19}$ and $\text{Mn}_{15}\text{Si}_{26}$) that have closely-related tetragonal crystal structures, with almost equal a and unusually long c lattice parameters, which simultaneously exhibit high positive Seebeck coefficients and low thermal conductivities, putting them as promising p -type TE materials. Some of the highest reported zT values were observed in the series of phases $\text{Ru}_{1-x}\text{Mn}_x\text{Si}_y$ ($0.14 \leq x \leq 0.97$, $1.584 \leq y \leq 1.741$), the alloy with $x = 0.90$ exhibiting $zT = 0.76$ at 874 K [77,78]. SiGe-additions in polycrystalline HMS affects the resistivity and thermal conductivity but not the Seebeck coefficient, and a maximum zT of 0.5 was achieved in $\text{MnSi}_{1.733-2\%}\text{SiGe}$ at 823 K [79]. Melt spinning and SPS on $\text{MnSi}_{1.75}$ creates in-situ nano-phase of MnSi, increasing the electrical conductivity and decreasing the thermal conductivity, and, consequently, zT reaches 0.62 at 800 K [80]. Polycrystalline Al-doped HMS prepared by melt-spinning combined with SPS have increased electrical conductivity and decreased thermal conductivity, the maximum $zT = 0.65$ being obtained at 850 K for $\text{Mn}(\text{Al}_{0.0015}\text{Si}_{0.9985})_{1.80}$ [81]. In Si-rich HMS materials, prepared by using simple solidification and SPS, a maximal $zT = 0.63$ at 723 K, was obtained [82,83]. MnSi_x ($x = 1.73, 1.75$ and 1.77) synthesized via mechanical ball milling and hot-press sintering showed that increasing Si contents yields a decrease in electrical conductivity and increase in Seebeck coefficient, $\text{MnSi}_{1.75}$ showing a maximum $zT = 0.55$ at 873 K [84]. Direct reaction Mn + Si in SPS leads to composite of tetragonal MnSi_x ($1.71 \leq x \leq 1.74$) and cubic MnSi with a zT of 0.34 at 870 K [85].

Thermoelectric properties of HMS prepared by MA and hot pressing seem to strongly depend on the preparation parameters: $zT = 0.28$ at 823 K [86] or $zT = 0.1$ at 723 K [83].

Orthorhombic β - FeSi_2 is an inexpensive semiconducting material where TE performance increase has been achieved. In the set of $\text{Fe}_{1-x}\text{Co}_x\text{Si}_{2+z}$ samples ($x = 0-0.08$; $z = -0.08-0.10$) prepared by hot uniaxial pressing the zT optimum (~ 0.20 at ~ 625 K) was found for $x = 0.06-0.07$ and $z = -0.04$ [87]. The effect of P substitution for Si, as an n -type dopant, on the TE properties of hot-pressed β - FeSi_2 leads to a zT almost the same as that of the conventional $\text{Fe}_{0.98}\text{Co}_{0.02}\text{Si}_2$ [88]. In Cr doped p -type and Co doped n -type β - FeSi_2 alloys a maximum zT of 1.1 at 845 K has been obtained by double doping in $\text{Fe}_{0.95}\text{Co}_{0.05}\text{Si}_{1.958}\text{Ge}_{0.042}$ [89]. β - FeSi_2 - TiB_2 composites with various amounts of TiB_2 , from 0 up to 30 vol.%, were prepared by hot pressing and had a low zT (at 750 K) = 0.15 [90], similar to Al- and Co-doped β - FeSi_2 fabricated by hot pressing technology ($zT = 0.182$ for $\text{Fe}_{0.95}\text{Co}_{0.05}\text{Si}_2$ at 900 K) [91].

The hexagonal CrSi_2 silicide has poorer reported TE properties than β - FeSi_2 . Ball milled and hot pressed CrSi_2 samples, despite Fe contamination, have a $zT = 0.2$ at 600 K [92]. $\text{Cr}_{1-x}\text{Mn}_x\text{Si}_{2-x}\text{Al}_x$ solid solutions exhibit $zT = 0.13$ at 625 K for $x = 0.10$ [93].

3.2 Antimonides

Antimonides have been regarded as potential TE materials since more than fifty years. In the Bi-Sb binary system a $\text{Bi}_{1-x}\text{Sb}_x$ solid solution is formed in all concentration range. $\text{Bi}_{1-x}\text{Sb}_x$ ($0.03 \leq x \leq 0.16$) has been considered one of the best n -type TE materials at 70–100 K temperatures, with $zT > 0.40$ measured on single crystals [94,95]. However, studies on polycrystalline samples show smaller zT values [96] and an influence of grain size and composition [97]. $\text{Bi}_{85}\text{Sb}_{15}$ alloys prepared by melt spinning and SPS show higher homogeneity, when compared with cast samples, and a $zT = 0.33$ at 120 K [98]. Nb and Ho doped $\text{Bi}_{1-x}\text{Sb}_x$ samples show n -type behavior, with increased TE properties [99,100]. Sn-doped Bi-Sb alloys are p -type semiconductors, with maximum $zT = 0.08$ at 200 K in $\text{Bi}_{0.885}\text{Sb}_{0.075}\text{Sn}_{0.04}$ [101] and $zT = 0.13$ at 240 K in $(\text{Bi}_{85}\text{Sb}_{15})_{0.975}\text{Sn}_{0.025}$ [102]. Pb% increase on $\text{Bi}_{85}\text{Sb}_{15-x}\text{Pb}_x$ leads also to p -type [103], the alloys synthesized by MA followed by pressure-less sintering having a maximum $zT = 0.11$ for $\text{Bi}_{85}\text{Sb}_{14}\text{Pb}_1$ at 210 K [104].

N -type $\text{Bi}_{1-x}\text{Sb}_x$ single crystals show large magnetothermoelectric figure of merit, which increases almost 3 times, to $zT = 1.28$ at ~ 220 K in $\text{Bi}_{88}\text{Sb}_{12}$, under a transverse field of 1.7 T [105]. A $zT = 0.41$ at 100 K is obtained in $\text{Bi}_{99}\text{Sb}_1$ in a field of 0.75 T [106].

M/T/M ($M = \text{Cu}$ or Ni and $T = \text{Bi}_{0.88}\text{Sb}_{0.12}$) composite materials have $zT = 0.44$ at 300 K, better than 0.26 in $\text{Bi}_{0.88}\text{Sb}_{0.12}$ [107]. In Bi-Sb based TE zT strongly decreases as the temperature increases, being interesting materials mainly for low temperature applications (see Sect. 3.6).

Strongly correlated semiconductors and Kondo insulators have been considered as potential TE materials for long time. Such materials have large *d*- or *f*-character of the electronic band structure close to the Fermi level that theoretically can lead to Seebeck coefficients (*S*) with large magnitudes. The strongly correlated semiconductor FeSb₂ exhibits a colossal Seebeck coefficient of $\sim -45000 \mu\text{V K}^{-1}$ at 10 K (see Sect. 3.6), but, due to a large thermal conductivity, zT is only 0.005 at 12 K [108].

Mn substituted CrSb₂ samples (with 0, 0.01, 0.03, 0.05Mn) are semiconductors with lower resistivity, slightly decrease of the Seebeck and strong decrease of the thermal conductivity, when compared with the undoped material, and $zT = 0.0125$ in Cr_{0.95}Mn_{0.05}Sb₂ at 313 K [109]. With Sb substitution of Sb, zT decreases [110].

Mg₃Bi₂ and Mg₃Sb₂, belonging to the zinc blend crystal structure family, were examined for the feasibility as medium temperature range thermoelectric elements [111]. They present medium PF, the last one showing relatively low thermal conductivity, which results in $zT = 0.55$ at 660 K [111]. Hot pressed samples of Mg₃Sb₂ with $zT = 0.21$ at 875 K were found to contain oxygen at the grain boundaries and to lose Mg and oxidize at temperatures above 900 K [112].

Thermoelectric properties of nanocrystalline (Mg_{1-x}Zn_x)₃Sb₂ alloys measured only up to 350 K [113] leads to low zT . Alloying with Bi decreases the thermal conductivity but keeps the PF low, the highest $zT = 0.4$ being realized for Mg₃BiSb at 825 K [114]. Preparation by SPS results in a substantial increase in Mg₃Sb_{2-x}Bi_x, to $zT = 0.6$ at 750 K [115].

β -Zn₄Sb₃ is a *p*-type material with a very low thermal conductivity and $zT = 1.3$ at 670 K, stable under argon up to 400 °C and under vacuum up to 250 °C [116,117].

Several methods have been used to prepare good TE β -Zn₄Sb₃ materials (zT of 0.8–1.2 at ~ 600 K), as vacuum melting [118], mechanical alloying [119] or direct synthesis by hot pressing [120]. Hot-pressed samples based on β -Zn₄Sb₃ with different amounts of ZnSb or Zn have lower zT , as both insertions have detrimental effect on PF and thermal conductivity [121]. Compacted samples of Zn₄Sb₃ have been prepared from the same synthesis batch by SPS and an apparent correlation of TE properties with sample density was found (zT from 0.08–0.32 at 300 K by changing the pressing conditions) [122]. ZnSb impurities cannot explain this variation, which may be caused by changes in Zn content and can have a larger effect on zT than doping [122]. The dimensionless figure of merit zT in the β -phase is found to be larger in the ingots prepared with Zn-rich starting composition than the Zn-poor one ($zT = 0.15$ at 300 K) [123]. A strong dependence of TE properties on Zn composition was confirmed, with a maximum $zT = 0.35$ at 340 K for the 56.52 at.% Zn material [124].

The high β -Zn₄Sb₃ TE efficiency results from the conjunction of a low thermal conductivity and the electronic structure of a heavily doped semiconductor. Interstitial Zn atoms and a partially occupied main Zn site, together with possible Sb disorder along the *c*-axis, are the main

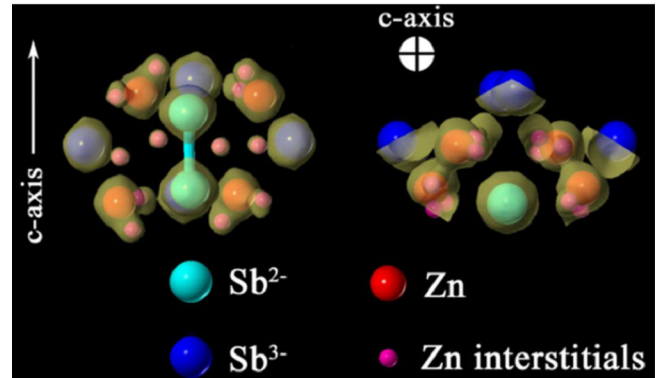


Fig. 7. Zn interstitials and Sb dimers in Zn₄Sb₃ (Ref. [125]).

reasons for the low value of thermal conductivity [125,126] (see Fig. 7). The ideal composition of the β -Zn₄Sb₃ is Zn₁₃Sb₁₀ (56.52 at.% Zn) and this compound can be seen as a Zintl phase [126].

β -Zn₄Sb₃ doping can lead to different behaviors. Zn₄Sb₃ was doped with 1 at.% Hg, but no zT change was observed up to 400 K [127]. In Te-doped Zn₄Sb_{3-x}Te_x prepared by hot-pressing zT values of 0.8 and 1.0 were obtained at 673 K for Zn_{4.08}Sb₃ and Zn₄Sb_{2.92}Te_{0.08}, respectively [128]. Ag doping in samples synthesized by melting and hot-pressing zT reaches 0.11 at 300 K in (Zn_{0.995}Ag_{0.005})₄Sb₃ [129], but in Zn₄Sb₃ bulk alloys with Ag, Pb or In prepared by induction melting and post-annealing only doping with Pb optimizes the TE performance (highest $zT = 1.12$ at 605 K for Pb_{0.02}Zn₄Sb₃) [130]. Sn seems not to enter the β -Zn₄Sb₃ structure, but a zT decrease is observed, most probably due to point defect phonon scattering induced by Sn inclusions [131]. Small iodine doping in Zn₄(Sb_{1-x}I_x)₃ ($0 < x \leq 0.015$) reduces the thermal conductivity and increases the Seebeck coefficient, the zT reaching 0.1 at 300 K in Zn₄(Sb_{0.995}I_{0.005})₃ [132]. High In concentrations (5, 10 and 15 at.%) lead to complex phase mixtures, which consist of β -Zn₄Sb₃ as the main phase and ZnSb, InSb and In as secondary phases. The maximum zT is 0.35 for the (Zn₄Sb₃)_{0.9}In_{0.1} at 680 K [133].

β -Zn₄Sb₃ + Cu₅Zn₃ bulk materials sintered by SPS with ZnSb and Cu₅Zn₈ impurities show highest $zT = 0.84$ for $m\text{Cu}_5\text{Zn}_3 \cdot n\text{Zn}_4\text{Sb}_3$ ($m/n = 1/200$) at 631 K [134].

Mo₃Sb₇ has a rather complex Ir₃Ge₇-type structure, displaying metallic and poor TE properties, but the partial Sb/Te substitution leads to a semiconducting behavior and a dramatic enhancement in the thermopower [135]. Mo₃Sb_{5.4}Te_{1.6} is a heavily doped semiconductor, with the high figure of merit of $zT = 0.80$ at 1050 K [136]. Mo₃Sb_{5.4}Te_{1.6} TE properties improvement has been made by 3*d*-metal doping, with Fe_{0.05}Mo₃Sb_{5.4}Te_{1.6} having the highest $zT = 0.31$ at 673 K and Ni_{0.06}Mo₃Sb_{5.4}Te_{1.6} achieving a $zT = 0.93$ at 1023 K [137,138]. Partial substitution of Mo by Ru significantly improves zT to 0.45 at 1000 K in Mo_{2.2}Ru_{0.8}Sb₇ [139].

The cubic *p*-type Yb₁₄MnSb₁₁ was the first complex Zintl phase (Fig. 8) with large figure of merit at high

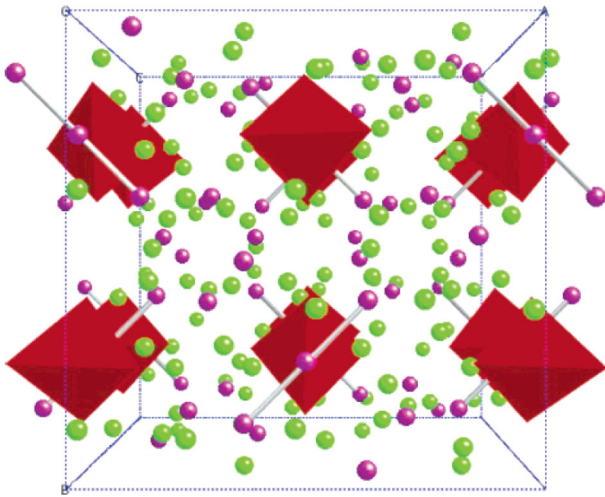


Fig. 8. Body centered crystal structure of $\text{Yb}_{14}\text{MnSb}_{11}$ (Ref. [140]).

temperatures (zT 0.8–1.0 at 1200 K), which is mainly due to the remarkably low thermal conductivity [140,141]. Substitutions with alkaline- and rare-earth elements, *d*-metals, and *p*-elements have been made to optimize the TE properties and good results were obtained for $\text{Yb}_{14-x}\text{Ca}_x\text{MnSb}_{11}$ ($x = 1, 2$, $zT \sim 0.92, 1.0$, respectively, at 1200 K) [142,143], $\text{Yb}_{14}\text{Mn}_{0.4}\text{Al}_{0.6}\text{Sb}_{11}$ ($zT = 1.1$ at 1223 K) [141], $\text{Yb}_{14}\text{Mn}_{0.6}\text{Zn}_{0.4}\text{Sb}_{11}$ ($zT > 1$ at 1275 K) [144] and $\text{Yb}_{14}\text{MnSb}_{10.93}\text{Te}_{0.07}$ ($zT > 1.1$ at 1240 K) [145].

Another family of Zintl antimonides that has good TE properties is $\text{Ca}_5\text{M}_2\text{Sb}_6$ ($\text{M} = \text{Al}, \text{Ga}, \text{In}$). $\text{Ca}_5\text{Al}_2\text{Sb}_6$ is a charge-balanced semiconductor with an extremely low lattice thermal conductivity [146]. Calcium substitution with sodium leads to the formation of free holes and to a transition from insulating to metallic behavior, the carrier concentration optimization giving a maximum $zT > 0.6$ at 1000 K for $\text{Ca}_{4.75}\text{Na}_{0.25}\text{Al}_2\text{Sb}_6$ [146]. $\text{Ca}_5\text{Ga}_2\text{Sb}_6$ and $\text{Ca}_5\text{In}_2\text{Sb}_6$ have reduced phonon velocities and improved carrier mobility relative to $\text{Ca}_5\text{Al}_2\text{Sb}_6$, which could give better zT [147]. In Zn-doped $\text{Ca}_5\text{Ga}_2\text{Sb}_6$ no improvement was observed due to the decreased band gap [148] but a modest zT increase relative to optimally doped $\text{Ca}_5\text{Al}_2\text{Sb}_6$ exists for Zn-doped $\text{Ca}_5\text{In}_2\text{Sb}_6$ (0.7 at 1000 K for $\text{Ca}_5\text{In}_{1.9}\text{Zn}_{0.1}\text{Sb}_6$) [149].

Sr_3GaSb_3 has a structure closely related to the $\text{Ca}_5\text{Ga}_2\text{Sb}_6$ -type. Zn-doped Sr_3GaSb_3 samples synthesized by ball milling followed by hot pressing show improved TE properties, with a maximum $zT = 0.9$ at 1000 K for $\text{Sr}_3\text{Ga}_{1-x}\text{Zn}_x\text{Sb}_3$ ($x = 0.0$ to 0.1) [150].

3.3 Tellurides

Tellurides contain several of the best TE materials discovered until now. Bi_2Te_3 - and PbTe -based ones show some of the highest values of figure of merit for bulk materials [151,152] and have been included in most of the review articles dedicated to TE, not being assessed here. How-

ever, many other tellurides with interesting TE properties exist.

Ag_2Te exists in three structural modifications: the monoclinic α -phase is stable below 418 K, the cubic β -phase is stable from 418 to 1075 K, and the γ -phase is stable from 1075 to 1233 K, the α - Ag_2Te having higher TE performance than that of β - Ag_2Te , with a maximum $zT = 0.27$ at 370 K [153].

The properties of the AgSbTe_2 are characterized by a larger thermoelectric power and lower Hall mobility than those of the $\text{Pb}_{1-x}\text{Sn}_x\text{Te}$. Early results pointed to $zT = 1.3$ at 720 K [154], but most probably in inhomogeneous samples (Widmanstätten precipitates of Sb_2Te_3) [155]. By using available thermal conductivity data, the estimated zT for plasma assisted sintering (PAS) AgSbTe_2 at 300 K was 0.29, larger than that of PAS- $\text{Pb}_{1-x}\text{Sn}_x\text{Te}$ at the same temperature [156]. Near single phase AgSbTe_2 has been prepared by high-pressure and high-temperature technique, with a large $zT = 1.07$ at 513 K [157,158]. Detailed studies on the precipitation of Ag_2Te in AgSbTe_2 have been made [159], the double-phased samples with Ag_2Te nanodots and nanoscale lamellar structures having a maximum $zT = 1.53$ at 500 K for $\text{Ag}_{0.84}\text{Sb}_{1.16}\text{Te}_{2.16}$ [160]. $(\text{Ag}_2\text{Te})_x(\text{Sb}_2\text{Te}_3)_{100-x}$ nanostructured bulk materials prepared by a sonochemical method and SPS show similar results [161]. TE properties of AgSbTe_2 were modified by doping, reaching 1.2 when doped with NaSe, and 1.05 with TlTe, at 400 K [162]. An enhancement of TE performance in Na-doped nonstoichiometric AgSbTe_2 samples, prepared by melt-quenching and SPS, was also observed ($zT = 1.50$ at 570 K for $\text{Ag}_{0.99}\text{Na}_{0.01}\text{SbTe}_{2.02}$) [163]. Se doping as well increases the AgSbTe_2 TE performance, but to a lesser extent [164,165]. Pure AgSbTe_2 porous samples prepared by melt-spinning and SPS have a $zT = 1.65$ at 570 K, which is much higher than in those prepared by traditional melting and slow-cooling [166].

The *p*-type ternary chalcopyrite semiconductor AgGaTe_2 shows a good TE performance that can be related to a heavy band-light band structure near the valence-band maximum, aided by the nearly isotropic transport. A $zT > 0.8$ at 850 K is observed [167], higher than $zT = 0.77$ at the same temperature in Ag deficient $\text{Ag}_{0.95}\text{GaTe}_2$ [168].

Studies on the $(\text{Cu}_2\text{Te})_{1-x}(\text{Ga}_2\text{Te}_3)_x$ series show that the nominally defect free phase CuGaTe_2 possesses the highest $zT \sim 1$ at 840 K and seems to continuously increase above this temperature [169].

Ga_2Te_3 is a *p*-type semiconducting compound with a defect zinc blend structure where one-third metal sublattice positions are unoccupied, the Ga ions and the structural vacancies being randomly distributed within the cation sub-lattice. It exhibits a low thermal conductivity, but the TE figure of merit is small due to its low carrier concentration [170]. $\text{Cu}_2\text{Ga}_4\text{Te}_7$ has the same defect zinc-blende crystal structure as Ga_2Te_3 , but a higher carrier concentration, the maximum zT being 0.64 at 940 K [171]. Cu and Sb co-substitutions for Te in Ga_2Te_3 also increase zT (0.5 at 700 K), mainly due to the reduction

of thermal conductivity and improvement of electrical conductivity [172].

Materials formed by alloying silver antimony telluride, AgSbTe_2 , with germanium telluride, GeTe , (TAGS) are known to have high zT values since the early 1960s [173], being reviewed in the middle 1990s [174] and early 2000s [175]. A p -type alloy $(\text{AgSbTe}_2)_{1-x}(\text{GeTe})_x$ with $x \sim 0.8-0.85$, called TAGS80, TAGS85, has a better zT (1.4–1.5), than for other x values, which is related to a minimum of thermal conductivity [176]. By partial substitution of Ag_2Te by Sb_2Te_3 in $(\text{GeTe})_{0.8}[(\text{Ag}_2\text{Te})_{0.4}(\text{Sb}_2\text{Te}_3)_{0.6}]_{0.2}$ a new p -type material with a $zT \sim 1.47$ at 700 K in a range of 200 K has been reported [177]. Rather similar properties have been observed by hot pressing of $\text{AgBiTe}_2\text{-GeTe}$, with a $zT = 1.32$ at 700 K for 3 mole% AgBiTe_2 [178], but with a smaller temperature range. The presence of nanoscale domains in TAGS may be one reason for the low lattice thermal conductivity and high zT values [179]. Studies on $(\text{GeTe})_x(\text{AgSbTe}_2)_{100-x}$ nanocomposites corroborate this possibility, with maximal $zT > 1.5$ at 720 K for $0.75 \leq x \leq 85$ [180]. The effect of atmosphere and doping on TE properties of TAGS was also analyzed. Studies made on TAGS-85 prepared by ball-milling in different atmospheres and sintered by SPS indicate better results for the Ar milled sample [181]. Doping TAGS-85 with magnetic rare earths form a dilute magnetic semiconductor, the localized moments contributing to increase the Seebeck coefficient and zT reaching a value higher than 1.5 at 730 K [182,183]. Hot pressed TAGS-80 and TAGS-85 were recently reported to show maximal zT values of ~ 1.75 and ~ 1.4 at 773 K, respectively [184]. TAGS85 has been used as p -leg in Radioisotope TE generators (RTG) for space applications.

The $(\text{PbTe})_x(\text{AgSbTe}_2)_{1-x}$ materials (known as LAST) are n -type high- zT systems with complex structure based on the NaCl lattice, where nanoinclusions exist. Albeit these materials were known since the late 1950's, their nanocomposite nature and high TE performance was only identified this century, in $\text{AgPb}_m\text{SbTe}_{2+m}$ samples prepared by melting followed by slow cooling, where nanoscale inhomogeneities were observed and a $zT = 2.2$ at 800 K for $m = 18$ was obtained [185]. Several studies were then performed in order to confirm the inhomogeneity character of the samples and identify the different domains [186–188]. However, later reports on the same (or closely related) materials show conflicting results, which reflect their complex nature and extreme sensitivity to composition and preparation conditions. As examples, we have the $\text{Ag}_{1-x}\text{Pb}_{18}\text{SbTe}_{20}$ prepared by solid-state reaction, which has a $zT = 0.33$ at 673 K with $x = 0.3$ [189], but $zT = 1.07$ at 673 K for $\text{Ag}_{0.6}\text{Pb}_{18}\text{SbTe}_{20}$ [190] and $\text{Ag}_{0.8}\text{Pb}_{18+x}\text{SbTe}_{20}$ fabricated by MA + SPS present a $zT = 1.37$ (673 K) [191], but if annealed for long time increases zT to 1.5 at 700 K [192]. Recent works on LAST prepared by different methods were reported to give similar high zT values [193]. The performance and nanoprecipitates formation in LAST were also subject

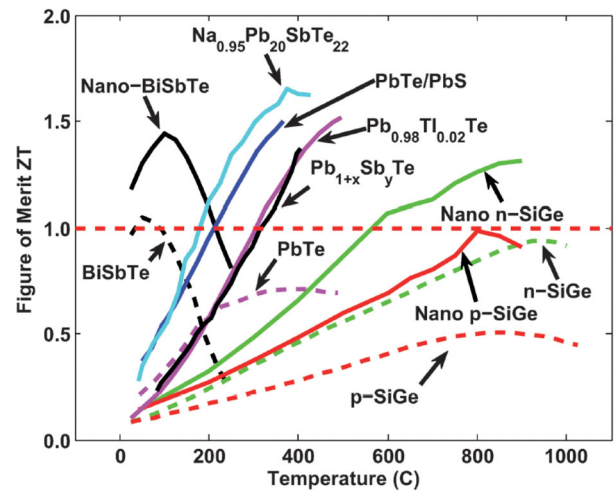


Fig. 9. zT versus temperature (dashed lines for bulk-, plain line for nano-structured-materials) (Ref. [13]).

of several theoretical investigations [194–198]. Sb addition was observed to tune the carrier concentration of $\text{AgPb}_{18}\text{Sb}_{1+x}\text{Te}_{20}$ alloys, with a maximum $zT = 1.33$ at 723 K for $x = 0.2$ [199,200], whereas Bi substantially reduces the Seebeck coefficient and lower zT values were obtained [199]. A general view of the high zT reached in nano-structured material versus temperature can be seen in Figure 9.

$\text{Ag}(\text{Pb}_{1-x}\text{Sn}_x)_m\text{SbTe}_{2+m}$ (also known as LASTT) are the p -type analogues of LAST materials. Similarly to LAST, they are also nanocomposites with high figures of merit. $zT = 1.4$ (625 K) was observed for $\text{Ag}_{0.5}\text{Pb}_6\text{Sn}_2\text{Sb}_{0.2}\text{Te}_{10}$ [201], and $zT = 1.1$ at 650–700 K was obtained in $(\text{AgSbTe}_2)_x(\text{Pb}_{0.5}\text{Sn}_{0.5}\text{Te})_{1-x}$ ($x = 0.05, 0.09, 0.2$) [202] and $\text{Ag}_{1-x}(\text{Pb}_{1-y}\text{Sn}_y)_m\text{Sb}_{1-z}\text{Te}_{m+2}$ [203], mainly due to the very low thermal conductivity.

In the p -type $\text{Na}_{1-x}\text{Pb}_m\text{Sb}_y\text{Te}_{m+2}$, silver-free sodium-substituted system (known as SALT) high zT values are also achieved. Natural nano-segregation of Na-Sb clusters is observed, leading to nanocomposites with very low thermal conductivity and a $zT = 1.7$ at 650 K for $\text{Na}_{0.95}\text{Pb}_{20}\text{SbTe}_{22}$ [204].

In-doped SnTe showed very large Seebeck coefficients and $zT \geq 1.0$ (700–800 K), which has been initially attributed to two In valence states [205] and recently to resonant levels created by In impurities inside the valence band [206].

$\text{Pb}_{0.5}\text{Sn}_{0.5}\text{Te}$ doped with In (few $10^{19}/\text{cm}^3$) sintered at a high pressure and high temperature (4.0 GPa and 800 or 900 °C), have a $zT = 0.75$ at 470 K for 0.07% In [207]. Sintering at the highest temperature improves the stability of the material.

P -type $\text{Ge}(\text{Sn},\text{Pb},\text{Te})\text{Te}$ alloys can have very low thermal conductivities, which arise from an ordered periodic nanostructure that results from a spinodal decomposition reaction, and the high $zT = 1.2$ at 723 K was obtained for $\text{Ge}_{0.5}\text{Sn}_{0.25}\text{Pb}_{0.25}\text{Te}$ [208]. Later works indicate that in $\text{Ge}_{0.5}\text{Pb}_{0.25}\text{Sn}_{0.25}\text{Te}$ the spinodal decomposition gives rise

to two Pb- and Ge-rich phases that leads to a significant decrease of the thermal conductivity, which is counter-balanced by a parallel drop on the electrical resistivity, resulting in a stable zT (0.95 at 673 K) [209].

The pseudo-binary alloys $\text{PbTe}_{1-x}\text{-SnTe}_x$ ($0 \leq x \leq 0.4$) doped with 0.02 mole% Ag concentration were prepared by SPS. The temperature at which the figures of merit reach a maximum increases with the mole fraction x . The property of the FGM (Functionally Graded Material) prepared by SPS is significantly improved as compared with those of any monolithic materials $\text{PbTe}_{1-x}\text{-SnTe}_x$ concerned [210].

The optimization of the carrier concentration of GeTe can be made by alloying with PbTe and/or Bi_2Te_3 doping, and zT 1.6–1.8 at 773 K were obtained in $\text{Pb}_{0.13}\text{Ge}_{0.87}\text{Te}$ with 3 mole% Bi_2Te_3 [211]. Phase separation reactions, by means of SPS consolidation and subsequently controlled heat treatments, enhance the TE properties of $\text{Ge}_{0.87}\text{Pb}_{0.13}\text{Te}$ and very high zT s ~ 2 are obtained [44].

GeTe TE properties can be also optimized by alloying with other compounds, and $zT = 1.54$ (700 K) and 1.15 (673 K) were obtained in $(\text{GeTe})_{0.82}(\text{Mn}_{0.6}\text{Sn}_{0.4}\text{Te})_{0.15}(\text{Bi}_2\text{Te}_3)_{0.03}$ and $(\text{GeTe})_{0.89}(\text{Ag}_8\text{GeTe}_6)_{0.11}$, respectively [212,213].

The properties of $(\text{Sn,Pb})(\text{Bi,Sb})_4\text{Te}_7$ hot press polycrystalline samples vary widely, from semiconducting to semi-metallic, with both n - and p -type conduction. They all have low thermal conductivity, the best zT value being observed for $\text{SnBi}_{2.5}\text{Sb}_{1.5}\text{Te}_7$ (0.55 at 400 K) [214].

Pressure has been used to explore the interaction parameters that determine the properties of the p -type BaBiTe_3 compound. Both thermoelectric power and electrical conductivity of BaBiTe_3 increase upon compression and, consequently, zT passes from ~ 0.1 to ~ 0.8 [215].

Several tellurides containing thallium show very low thermal conductivities, having potential as TE materials. Cu doping resulted in a net increase of the hole concentration of AgTlTe , improving the PF while keeping the thermal conductivity extremely low, and leading to an enhancement of the TE figure of merit ($zT = 0.6$ at 550 K for $\text{Ag}_{0.6}\text{Cu}_{0.4}\text{TlTe}$) [216]. First principles calculations on AgTlTe point to $zT = 0.5$ at 300 K for both holes and electrons [217].

A systematic investigation of TE properties of TlMTe_2 ($M = \text{Ga}, \text{In}, \text{Tl}$) showed that the low thermal conductivity in many thallium tellurides cannot be explained solely by the presence of Tl: very low thermal conductivities were observed in the Ga and In compounds (and consequently, reasonable $zT \sim 0.45$ at 850 K), while TlTe exhibits an extremely high value [218]. In p -type TlMTe_2 ($M = \text{Sb}, \text{Bi}$) polycrystalline samples, TlSbTe_2 has a higher zT (0.87 at 715 K) than with Bi [219].

Both p -type compounds Tl_2MTe_5 ($M = \text{Ge}, \text{Sn}$) have very low thermal conductivity (complex structure) and high zT (0.6 at 300 K, 0.85 at 400 K) [220]. Tl_9BiTe_6 has a $zT \sim 1.2$ at 500 K, which is mainly due to the extremely low thermal conductivity [221]. Ag_9TlTe_x ($5 \leq x \leq 6$) has also an extremely low thermal conductivity and high zT for $x > 5$ ($zT = 1.23$ at 700 K in Ag_9TlTe_6) [222].

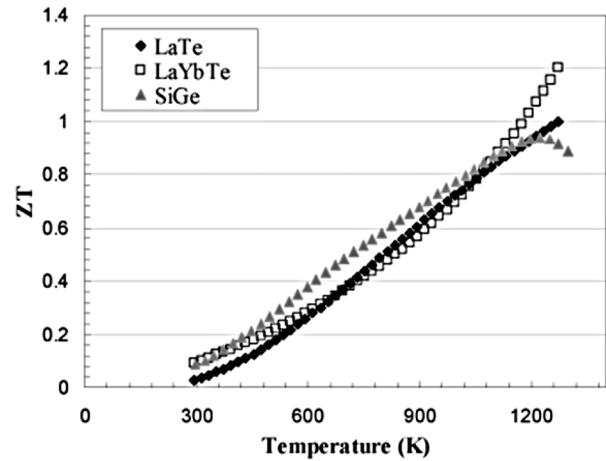


Fig. 10. Effect of Yb doping on zT of LaTe and comparison with SiGe (Ref. [228]).

However environmental constraints limit the interest of such Tl-based compounds. A review on the TE properties of thallium-based compounds and tellurides of other group 13 elements was presented [223].

Studies made on $\text{In}_4(\text{Se}_{1-x}\text{Te}_x)_3$ alloys prepared by melt quenched + SPS indicate that Te substitution can effectively reduce the thermal conductivity down to that of In_4Te_3 , while maintaining the PF, and a $zT = 0.25$ at 600 K was observed for In_4Te_3 [224].

Early studies on the La-Te system indicated that the composition of interest for TE materials is $\text{La}_{3-x}\text{Te}_4$, where x is the number of lanthanum vacancies per formula unit and is restricted to $0 \leq x \leq 1/3$ [225]. The electron concentration is coupled to the lanthanum vacancy concentration and when $x = 1/3$ the stoichiometric can be written as La_2Te_3 . Controlling the Te to La stoichiometry is thus vital to achieving the optimum self-doping level for the highest dimensionless zT value.

N -type $\text{LaTe}_{1.46}$ has been the subject of numerous studies due to the high value of zT ($zT = 0.96$ at 1200 K) [226]. $\text{La}_3\text{Te}_{4-x}$ prepared by MA and hot press has a $zT = 1.1$ at 1275 K [227], the value increasing by Yb doping ($zT = 1.2$ at 1200 K) [228] (Fig. 10).

Sb_2Te_3 has a low Seebeck coefficient arising from the high hole concentration generated by Sb antisite defects, but alloying and/or doping can compensate or suppress them. $\text{Cu}_x\text{Bi}_{0.5}\text{Sb}_{1.5-x}\text{Te}_3$ ($x = 0-0.4$) alloys prepared by cold pressing show strong influence of TE properties on the Cu concentration, the maximum figure of merit, $zT = 0.74$ at 442 K, corresponding to $x = 0.05-0.1$ [229]. Studies on $(\text{Cu}_4\text{Te}_3)_x(\text{Bi}_{0.5}\text{Sb}_{1.5}\text{Te}_3)_{1-x}$ materials fabricated by SPS, reveal very high electrical conductivity, low lattice thermal conductivity, the Seebeck coefficient linearly increasing with temperature and a maximum $zT = 1.26$ at 474 K for $x = 0.025$ [230]. Silver alloys also have good TE properties, $(\text{Ag}_{0.365}\text{Sb}_{0.558}\text{Te})_{0.025}(\text{Bi}_{0.5}\text{Sb}_{1.5}\text{Te}_3)_{0.975}$ reaching $zT = 1.1$ at 478 K [231]. Ga_2Te_3 substitution for $\text{Bi}_{0.5}\text{Sb}_{1.5}\text{Te}_3$ leads to a performance similar to that of

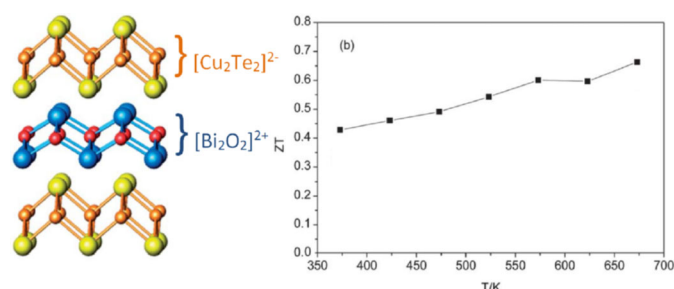


Fig. 11. Structure and high zT value in the oxy-telluride BiO-CuTe (Ref. [239]).

$\text{Ag}_{0.365}\text{Sb}_{0.558}\text{Te}$ and to a $zT = 1.0$ at 336 K for the $x = 0.1$ molar fraction [232].

The p -type nanostructured Ge-doped $\text{Sb}_{100}\text{GeTe}_{150}$ alloy has $zT = 0.84$ at 492 K [233], whereas in the nanostructured series $\text{Ga}_m\text{Sb}_n\text{Te}_{1.5(m+n)}$ a maximum $zT = 0.98$ at 482 K is observed for the alloy with $m:n = 1:10$ [234], which is mainly due to the substantial reduction in the lattice thermal conductivity.

Subatomic percent S doping is very effective in suppressing antisite defect formation and $zT = 0.95$ at 423 K was reached for 0.1–0.5 at.% S doped Sb_2Te_3 [235].

$\text{Nb}_3\text{Sb}_2\text{Te}_5$ crystallizes in a noncentrosymmetric variant of the Ir_3Ge_7 type, the forty atoms per unit cell and its varied mixture of atoms yielding a complicated structure, suggesting that compounds with this structure type may exhibit low thermal conductivity and hence high zT values. Various compositions of $\text{Nb}_3\text{Sb}_x\text{Te}_{7-x}$ have been studied, but TE properties are compromised by compensating n -type and p -type carriers [236].

Properties of hot press polycrystalline samples of $(\text{Sn,Pb})(\text{Bi,Sb})_4\text{Te}_7$ vary widely from semiconducting to semi-metallic, with both n - and p -type conduction, all have low thermal conductivity. The best zT value obtained was 0.55 at 400 K for $\text{SnBi}_{2.5}\text{Sb}_{1.5}\text{Te}_7$ [214]). SnBi_4Te_7 exhibits both n -type conductivity (Te deficiency and Sn or Bi excess) and p -type conductivity (Te excess and Sn or Bi deficiency), whereas only n -type conductivity samples were obtained for PbBi_4Te_7 [237].

Oxytellurides have recently emerged as potential TE materials. Electron doping into Cd_3TeO_6 single crystals was carried out by either the introduction of oxygen vacancies, or the atomic substitution of In for Cd, with $zT = 0.3$ at 300 K [238]. Much higher values were lately obtained in BiOCuTe , with a $zT = 0.66$ at 673 K, the maximum temperature investigated, due to an extremely low lattice thermal conductivity of $0.5 \text{ W m}^{-1} \text{ K}^{-1}$ [239] (Fig. 11).

3.4 Sulfides, selenides

The PF of TE oxides is generally too low, so increasing the covalency by replacing O by the S or Se chalcogenide is one way to improve it [240,241]. Indeed, PbS has been considered for a long time a good material for thermoelectric energy conversion [242,243] and other selenides and sulfides have been studied and optimized in the last century for thermoelectrics.

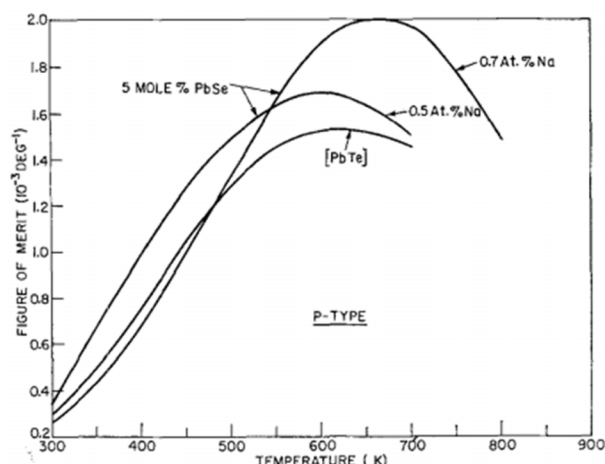


Fig. 12. Temperature dependence of zT for p -type PbTe-PbSe alloys, the curve for PbTe is shown for comparison (Ref. [245]).

Dilute alloys PbTe-GeTe are n -type materials with figures of merit 35 to 40 times greater than PbTe in the 300–800 K temperature range [244]. In order to produce p -type with high zT , PbSe-PbTe alloys have been studied. A maximum zT was observed for alloys containing 5 to 15 mole% PbSe, doped with at least 0.7 at.% Na [245]. Conversely to the case of PbTe-GeTe, the increase of zT (to ~ 1.4 at ~ 700 K, see Fig. 12) is mainly due to an enhancement of PF and not to the decrease of the thermal conductivity.

Single crystals of n -type PbSe Cl-doped via PbCl_2 show a maximum $zT = 0.8$ at 700 K for a carrier concentration of $\sim 1.5 \times 10^{19} \text{ cm}^{-3}$ (0.20 mole% PbCl_2). The involvement of optical phonons in conducting heat at high temperatures implies that in PbSe the lattice thermal conductivity at 700–900 K is higher, in relative terms, than in PbTe, where optical phonons are less important [246].

Thermoelectric properties of PbSe doped with Ga, In, and excess Pb, maintaining the n -type, have been recently reported as a function of carrier density and temperature. There is a general perception in the literature that n -type PbTe is a better thermoelectric material than PbSe at all temperatures, but this work shows that at 900 K the doped PbSe ($zT = 0.9$) outperforms PbTe [247].

Digenite, $\text{Cu}_{1.8}\text{S}$, is a semiconductor with high electrical conductivity, but with low Seebeck coefficient ($\sim 10 \mu\text{V K}^{-1}$) and high thermal conductivity, not being directly suitable for thermoelectric applications [248]. However, the $\text{Cu}_{1.8}\text{S}$ sample with a second $\text{Cu}_{1.96}\text{S}$ phase and micro pores shows its maximum zT value 0.5 at 673 K, which is a high value for p -type sulfide thermoelectric materials [249]. The closely related copper (I) selenide, Cu_2Se , is a mixed ion-electron conductor that was considered in the 1960–70's to be a competitive thermoelectric material (Ref. [250] and references therein). This material has a low thermal conductivity and $zT = 1.2$ was found for $\text{Cu}_{1.97}\text{Ag}_{0.03}\text{Se}$ at 1000 K, due to transverse phonon modes being suppressed by fast relaxation time [250]. More recently, Cu_2Se was reported to have a high figure of merit, $zT > 1$ at 400 K, which was connected

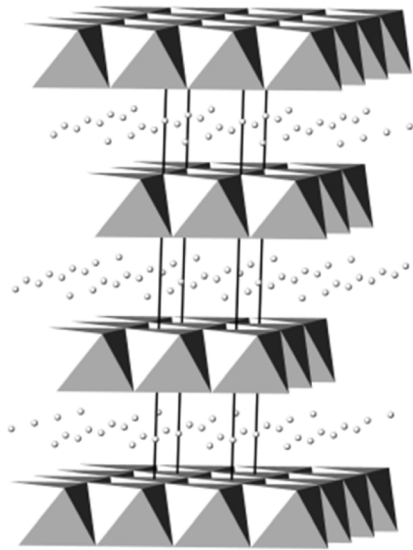


Fig. 13. Crystal structure of AgCrSe₂ with CdI₂-type layers (CrSe₆ octahedra) and disordered Ag cations over 2 sites (Ref. [253]).

to a second-order structural phase transition that leads to a super-ionic conducting phase [251,252]. Despite its zT , the poor stability and chemical reactivity with contacts of these compounds prevent their use in devices [250].

Other superionic phases that have also been considered as potential thermoelectric materials are the layered compounds CuCrSe₂ and AgCrSe₂. Their structure can be described as CdI₂-type layers of CrSe₂ in which the Cr are in a distorted octahedral coordination by Se anions, the interlayer spaces being filled by Cu or Ag cations. A crystallographic transition occurs at 400–475 K above which the cations are disordered, which leads to low thermal conductivities [253]. This description resembles that of many good TE materials that show a clear separation between the region of electronic conduction and the zone of phonon scattering. Recent electrical transport and thermal conductivity measurements on CuCrSe₂ show strong properties dependence on the preparation conditions and point to the possibility of very high figures of merit ($zT = 2$ at 300 K in a textured sample) [254]. The sensitivity on the preparation history and composition as been reflected on later works, where zT values between 0.11 and 1 have been reported [255–258]. The isostructural silver selenide, AgCrSe₂, also presents large values of zT (up to 0.8 at 700 K) [253,259] (Fig. 13).

The PF is very much influenced by the Seebeck behavior [259] (Fig. 14).

TiS₂ and TiSe₂ are layered compounds that crystallize in the CdI₂-type structure and where intercalated species between the layers can also be inserted. Ti_{1+x}S₂ has been studied for TE properties and $zT = 0.34$ at 663 K in Ti_{1.008}S₂ was found for a textured sample [260]. The TiS_xSe_{2-x} solid solutions were explored and a maximum $zT \approx 0.4$ at 673 K was reached for TiS_{1.5}Se_{0.5}, mainly due to the decrease of the thermal conductivity [261]. After Co doping the zT of TiS₂ is very low (0.03 at 310 K

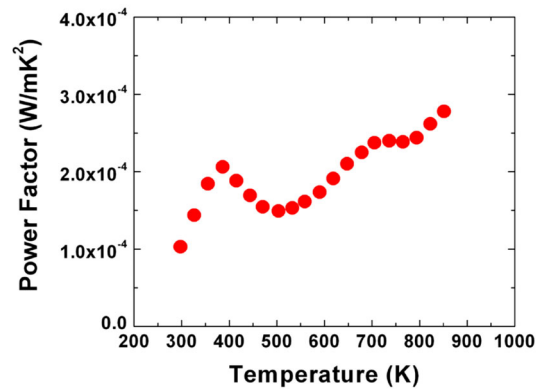


Fig. 14. Power factor versus temperature for AgCrSe₂.

for Co_{0.3}Ti_{0.7}S₂ [262]), but intercalation of Cu ions using SPS leads to a much better value ($zT = 0.45$ at 800 K) in Cu_{0.02}TiS₂ [263], as it decreases both the electrical resistivity and the thermal conductivity. The influence of Cu intercalation on the electrical and thermal transport properties of TiSe₂ has been studied and a significant raise of the PF and reduction of the thermal conductivity with increasing cation content was observed, but a low $zT = 0.104$ at 300 K was still obtained [264,265]. Similar results were found for co-intercalated Ni_xTi_{1+y}Se₂ samples sintered by SPS, with an estimated $zT \sim 0.1$ at 550 K [266].

Wet-chemistry Li intercalation process in layered ZrSe₂ single crystals induced additional charge carriers and structural disorder that favorably affected the thermoelectric properties of the material and zT reached 0.26 at 300 K [267].

Misfit layered compounds based on TiS₂ have also attracted considerable interest as potential TE materials (Fig. 15). Here the TiS₂ layer can provide high PF, while the intercalated layer forms with TiS₂ a modulated structure which can suppress the transport of phonons. The properties of a single-crystalline [Sn₂S₂]_pTiS₂ misfit layered material were first investigated and PF as high as 12×10^{-4} W/K² m were found at room temperature [268]. Later studies on (SnS)_{1.2}(TiS₂)₂ indicated zT exceeding 0.35 at 670 K [269], but lower values were also reported for the same material ($zT \sim 0.2$ at 673 K) [270]. A series of misfit layer compounds of composition (MS)_{1+x}(TiS₂)₂ (M = Pb, Bi, Sn) were investigated, being promising thermoelectric materials (zT values of 0.28 ~ 0.37 at 700 K), but with too high carrier concentrations [271].

Attempts to decrease the carrier concentration by doping electron acceptors were made by substituting Mg²⁺ for Ti⁴⁺ in the host layers ((BiS)_{1.2}(Mg_xTi_{1-x}S₂)₂) or by substituting Ca²⁺ and Sr²⁺ for Bi³⁺ in the phonon barrier ((Bi_{1-x}(Ca,Sr)_xS)_{1.2}(TiS₂)₂), but with no significant success [272]. Although the chromium substitution did not result in higher power factor, its low total thermal conductivity contributed to some increase in zT [273]. In the misfit-layered sulfides [Ln₂S₂]_pNbS₂ (Ln = lanthanides), zT only reaches 0.11 at 300 K, which is mainly due to their small Seebeck coefficient [274].

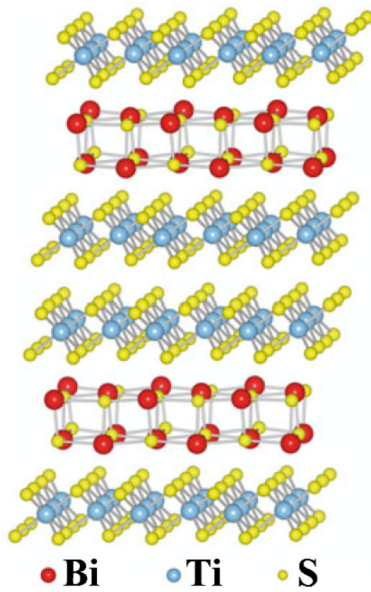


Fig. 15. Superlattice structure of $(\text{BiS})_{1.2}(\text{TiS}_2)_2$ misfit layer sulfide.

LnS_x ($1.33 \leq x \leq 1.5$) rare earth sulfides have been studied from the 60's for thermoelectrics, with figures of merit as high as $zT = 0.75$ [275–278]. In the high temperature range, the γ -phase $\text{La}_{3-x}\text{S}_4$ behaves as an extrinsic semiconductor, whose degenerate carrier concentration is controlled by the stoichiometric ratio of La to S, and a zT of 0.7 at 1400 K was obtained [277]. Sm, Eu and Yb additives, as well as Ca, Sr and Hg, did not improve zT . Thermal conductivity measurements for GdSe_x ($x = 1.49$ – 1.495) were a factor of two or three lower than those measured on LaS_x , and resulting figures-of-merit greater than one (1.17 in $\text{GdSe}_{1.49}$ at 1173 K) were reported, indicating $\text{GdSe} \sim 1.49$ as an excellent thermoelectric material [226]. A zT close to 1.0 ($zT = 0.93$) was also reported in $\text{NdS}_{1.50}$ at 1073 K. In Ln_2S_3 (Ln = Gd and Tb) the PF increases with the density and zT with the decreasing S content [279].

The synthesis and pressure assisted sintering of the ternary rare-earth sulfides LnGdS_3 (Ln: Pr, Nd) give the highest figure of merit ($zT = 0.51$) for $\text{NdGd}_{1.02}\text{S}_3$ at 950 K [280], much lower than in $\text{NdS}_{1.50}$. Compounds of the type $\text{La}_{3-x}\text{M}_x\text{S}_4$, where M is Ca, Sr or Hg and x ranges from 0.1 to 0.9, were prepared by the pressure assisted reaction sintering. Samples are n -type and have good PF [278]. $\text{La}_{2.2}\text{Ca}_{0.8}\text{S}_4$ has a maximum value of $zT = 1.6$ at 973 K and the substitution stabilizes the structure at high temperature [281]. The cubic SmEuGdS_4 is a p -type compound but with a high resistivity, not being suitable for TE [280].

Sulfides and selenides containing alkaline or transition metals have as well been considered as potential high performance TE materials. The $\text{KBi}_{6.33}\text{S}_{10}$ and $\text{K}_2\text{Bi}_8\text{S}_{13}$ ternary bismuth sulfides were originally found to have small thermal conductivities, but too low thermoelectric power for practical applications [282]. Considerable better performance was obtained for the isostructural selenide,

$\beta\text{-K}_2\text{Bi}_8\text{Se}_{13}$, where a $zT = 0.22$ at 300 K was found [283]. By alloying with S and optimizing the composition and preparation conditions was possible to increase even more the figure of merit, up to 0.58 at 623 K [284].

The thermoelectric properties of sulfides and selenides with structures derived from the zinc blende type have also been recently studied.

Chalcopyrite CuFeS_2 nanocrystals with a diameter of 6.4 nm were synthesized using a facile solution-phase method. The nanograin size leads to small thermal conductivities and the quantum confinement to large PF, giving a maximum zT value of 0.264 at 500 K, strongly improved as compared to the bulk material [285]. Carrier-doping of chalcopyrite with Fe and Zn ($\text{Cu}_{1-x}\text{Fe}_{1+x}\text{S}_2$ ($0 \leq x \leq 0.3$) and $\text{Zn}_{0.03}\text{Cu}_{0.97}\text{FeS}_2$) increases the PF and decreases the thermal conductivity, giving a $zT \sim 0.07$ at 400 K but still increasing with the T rise [286,287]. The decreasing S content in CuFeS_{2-x} results in an electrical resistivity and thermal conductivity decrease, with a maximum $zT = 0.21$ at 573 K for $\text{CuFeS}_{1.80}$ [288].

Type p -diamond like $\text{Cu}_2\text{Ge}_{1+x}\text{Se}_3$ and Cu_2SnSe_3 (nanocrystals) consolidated by SPS have low thermal conductivity, high mobility and a $zT = 0.3$ at ~ 700 K [289,290], which could probably be improved by doping. Pellets made from Cu_2GeSe_3 nanoparticles, with a mixture of wurtzite and zinc blende structures, present maximum $zT = 0.27$ at 723 K [291]. $\text{Cu}_2\text{Ga}_{0.1}\text{Ge}_{0.9}\text{Se}_3$ also has a quite small power factor that leads to values of $zT = 0.5$ at 750 K, due to a very low thermal conductivity [292]. Ab initio calculations on Cu_2SnX_3 ($X = \text{Se}, \text{S}$) pointed to the possibility of obtaining $zT \sim 1$ [293]. Indeed, higher values were obtained for $\text{Cu}_2\text{Sn}_{0.90}\text{In}_{0.10}\text{Se}_3$, with $zT = 1.14$ at 850 K [294].

Cu_3AsSe_4 and Cu_3SbSe_4 have been reported to be good candidate TE materials with anomalously low thermal conductivities [295] and high carrier mobility at room temperature.

Similar characteristics in quaternary chalcogenides of $\text{Cu}_{2.10}\text{Cd}_{0.90}\text{SnSe}_4$, $\text{Cu}_{2.1}\text{Zn}_{0.9}\text{SnSe}_4$ and $\text{Cu}_2\text{ZnSn}_{0.9}\text{In}_{0.1}\text{Se}_4$, with a distorted diamond like structure and large gap, leads to high zT , respectively 0.65 at 700 K [296], 0.9 at 860 K [297] and 0.95 at 850 K [298]. Pellets made from $\text{Cu}_{2.15}\text{Cd}_{0.85}\text{SnSe}_{3.9}$ nanoparticles reached $zT = 0.71$ at 685 K [299]. By doping Sn in the Sb site zT reaches 0.75 at 673 K ($\text{Cu}_3\text{Sb}_{0.975}\text{Sn}_{0.025}\text{Se}_4$) [300], while Bi-doping gives 0.7 at 600 K ($\text{Cu}_3\text{Sb}_{0.98}\text{Bi}_{0.02}\text{Se}_4$) [301].

Compounds of the form $\text{Cu}_3\text{Sb}_{1-y}\text{Ge}_y\text{Se}_{4-x}\text{S}_x$ have zT in excess of 0.8 at 650 K, with a maximum value of 0.89 for $x = 1.2$, $y = 0.03$ due to additional phonon scattering by the disordered arrangement of Se and S [302].

Preliminary works on polycrystalline $\text{Cu}_{10}\text{Tr}_2\text{Sb}_4\text{S}_{13}$ (Tr = Mn, Fe, Co, Ni, Cu, Zn) tetrahedrite samples revealed rather high $zT = 0.15$ at 340 K for the Ni material [303]. $\text{Cu}_{11.5}\text{Zn}_{0.5}\text{Sb}_4\text{S}_{13}$ exhibits a $zT = 0.95$ at 720 K, highlighting the potential of tetrahedrites as a high-temperature TE material [304]. A dimensionless thermoelectric figure of merit of 0.7 at 665 K was obtained for $\text{Cu}_{10.5}\text{Ni}_{1.5}\text{Sb}_4\text{S}_{13}$, which is a considerably high value

among p -type Pb-free sulfides [305]. The direct use of the tetrahedrite natural mineral provided a low cost mean of producing high conversion efficiency TE materials with zT close to unity at 723 K [306].

The Co-Sb-S ternary system has been explored and CoSbS was found to exist [307]. Its electrical transport properties characterization indicates a potential TE material [307]. Polycrystalline samples of nominal composition $\text{Co}_{1-x}\text{Ni}_x\text{SbS}$ with $x = 0, 0.01, 0.03, 0.06$ densified by pressure assisted sintering are n -type with a rather large zT of 0.35 at 772 K, even though the thermal conductivity is large (7–8 W/m K at 300 K), which opens opportunities for improvements by appropriate doping [308]. From calculated band structure Fe-based sample is also semi-conducting and could be of interest for TE but Ni-based is metallic.

Thermoelectric properties of CuSbSe_2 and $\text{CuM}_{0.02}\text{Sb}_{0.98}\text{Se}_2$ ($M = \text{Ti, Pb}$) have been studied showing small zT values at 300 K but strong reduction of the thermal conductivity and zT improvement by Ti substitution, whereas with Pb the Seebeck coefficient decreases [309]. The structural and transport properties in AgSbTe_2 - AgSbSe_2 system were investigated and a high value of $zT = 0.65$ at 520 K was observed for the $\text{AgSbSe}_{0.25}\text{Te}_{1.75}$ sample [164]. The zT increases to 0.51 at 550 K in $\text{AgBi}_{0.5}\text{Sb}_{0.5}\text{Se}_2$ by the formation of solid solution, and then further increases to 1.07 at 550 K by the formation of solid-solutioned homojunction [310]. In AgBiSe_2 a phase transition occurs at ~ 580 K and the high zT value of 1.5 was obtained around 700 K [311]. The value of $zT = 1$ at 773 K has been recently observed in $\text{Ag}_{0.96}\text{Nb}_{0.04}\text{BiSe}_2$ [312].

In Pb-filled Chevrel-phase sulfides $\text{PbMo}_6\text{S}_{7.8}$ a low lattice thermal conductivity is induced by the complex crystallographic structure, but zT stays low (0.08 at 850 K) [313]. In $\text{Cu}_x\text{Mo}_6\text{S}_8$ the increase in Cu content increases the Seebeck coefficient and electrical resistivity, whereas the thermal conductivity decreases, leading to the highest zT (0.4) for $\text{Cu}_4\text{Mo}_6\text{S}_8$, at 950 K [314].

In selenide Chevrel phases, small inserted atoms in the cavities of the Mo_6Se_8 structure usually show large thermal parameters, which indicate that they move around and can significantly scatter the phonons. $zT = 0.6$ (1150 K) has been obtained in the $\text{M}_x\text{Mo}_6\text{Se}_8$ ($M = \text{Cu, Cu/Fe, Ti}$) series for $\text{Cu}_{3.1}\text{Mo}_6\text{Se}_8$ [315] and of 0.22 at 800 K in TiMo_6Se_8 [316]. No improvement of zT in $(\text{Cu}_y\text{Mo}_6\text{Se}_8)_{1-x}(\text{Mo}_4\text{Ru}_2\text{Se}_8)_x$ as compared to $\text{Cu}_{3.1}\text{Mo}_6\text{Se}_8$ was observed [317].

Mo clusters with a nuclearity higher than six can also be obtained and derive from the one-dimensional transface sharing of Mo_6 octahedra. $\text{Ag}_x\text{Mo}_9\text{Se}_{11}$ ($x \sim 3.6\text{--}3.8$) show p -type conduction and very low lattice thermal conductivity that give rise to $zT = 0.65$ at 800 K, making this family of materials promising for TE applications [318].

The $\text{In}_4\text{Se}_{3-\delta}$ ($\delta = 0.65$) single crystalline n -type material achieves $zT = 1.48$ at 705 K [319]. Slightly higher values ($zT = 1.53$ at 698 K) were obtained for $\text{In}_4\text{Se}_{2.67}\text{Cl}_{0.03}$ chlorine-doped single crystals, but with a larger zT in a wide temperature range [320], while iodine-substituted

$\text{In}_4\text{Se}_{2.32}\text{I}_{0.03}$ crystals exhibits $zT = 0.33$ at 300 K and $zT = 1.0$ at 660 K [321]. However, measurements made on polycrystalline materials resulted in lower zT values due to the anisotropic structure [322,323]. The maximum zT of polycrystalline $\text{In}_4\text{Se}_{2.7}\text{Cl}_{0.03}$ reaches ~ 0.67 at 673 K, which is an improvement when compared with the undoped compound [324]. Cationic substitution on $\text{In}_{4-x}\text{M}_x\text{Se}_{2.95}$ ($M = \text{Na, Ca, Zn, Ga, Sn, Pb}$; $x = 0.1$) decreases the zT values, probably due to a weakening of the Peierls distortion effect on the thermal properties of $\text{In}_4\text{Se}_{3-x}$ [325]. Incorporation of Cu into the In_2Se_3 lattice results in a change in morphology from amorphous-like structure (In_2Se_3) to a visible polycrystalline form, which enhances the lattice thermal conductivity, but also reduces the bandgap and higher zT values are obtained (0.55 for $\text{In}_{1.8}\text{Cu}_{0.2}\text{Se}_3$ at 846 K) [326]. The textured composite with elemental In embedded in the In_4Se_3 matrix has maximum figure of merit $zT = 0.9$ at 700 K [327].

The measured band-gap of AgIn_5Se_8 is 1.25 eV, smaller than that of In_2Se_3 , hence it is a more applicable TE material than In_2Se_3 . A gradual microstructure change was observed from twinning to nanoparticle-dominated structure as the annealing time increases to 100 days at 180 °C and zT reaches 0.72 at 863 K in AgIn_5Se_8 with this microstructure modulation [328].

The low dimensional structure $\text{Tl}_x\text{Cr}_5\text{Se}_8$ pseudohollandite has a large Seebeck coefficient at 800 K in spite of the relatively low resistivity values. Moreover, the thermal conductivity is also small, leading to $zT = 0.5$ at 800 K [329].

P -type $\text{Bi}_{1-x}\text{Sr}_x\text{CuSeO}$, a layered oxyselenide, evidence high electrical conductivity and Seebeck coefficient, which, combined with the low thermal conductivity, leads to $zT = 0.76$ at 873 K for $\text{Bi}_{0.925}\text{Sr}_{0.075}\text{CuSeO}$ [330]. The pure BiCuSeO is also a promising TE material: MA powders consolidated by SPS show a $zT \sim 0.7$ at 773 K, mainly due to the decrease of the thermal conductivity [331]. Bi^{3+} substitution by alkali metals (Mg, Ca, Sr and Ba) leads to the optimization of the charge carrier concentration and a slight decrease of the lattice thermal conductivity (through point-defect scattering of the phonons), resulting in a maximum $zT = 1.1$ at 923 K for $\text{Bi}_{0.875}\text{Ba}_{0.125}\text{CuSeO}$ [332–336].

3.5 Other promising materials

Several other materials have been considered promising for TE applications. Boron-based ones have been considered for a long time to be of interest for TE ([337] and references therein). Divalent hexaborides (CaB_6 , SrB_6 and YbB_6) have large and negative Seebeck coefficients (–100 to $-270 \mu\text{V/K}$ at 1073 K), giving $zT = 0.3$ at 1073 K for SrB_6 , while those of trivalent and intermediate-valent hexaborides (CeB_6 and SmB_6) are small [338].

Investigation of the thermoelectric properties was carried out for the homologous series of LnB_{17}CN , $\text{LnB}_{22}\text{C}_2\text{N}$, and $\text{LnB}_{28.5}\text{C}_4$ ($\text{Ln} = \text{lanthanide}$). SPS was found to be effective in the densification of samples, when

compared to conventional hot press and cold press techniques, but PF and zT stay very low [339,340]. zT is also low at 1000 K in TbB₄₄Si₂, ErB₄₄Si₂, YbB₄₄Si₂ [341]. In B-rich silicon borides (B content range 90.0 to 97.0 at.%) prepared by arc-melting and SPS, the largest zT value, reached 0.2 at 1100 K [342].

In composite B₄C + SiB_{*n*} (*n* = 4, 6, 14) heat treatment modifies the microstructure and TE properties, and a zT of 0.29 at 1100 K has been obtained [343].

Using magnetron sputtering to produce large quantities of Si/Si_{0.8}Ge_{0.2} and B₄C/B₉C superlattices, quantum well films with up to 1000 layers were deposited with high expected zT at low cost [344]. A $zT > 4$ has been reported for systems of such multilayered Si/SiGe *n*-legs and B₄C/B₉C *p*-legs [345].

The TE properties of FeGa₃ polycrystalline samples have been evaluated above room temperature and a semiconductor-like behavior has been observed, but the maximum zT reaches only 0.04 at 973 K [346]. FeGa₃ later studies indicated a metallic-like behavior and *p*-type dominated TE transport, which has been ascribed to off-stoichiometric effects [347]. Measurements on single crystals confirm the semiconducting character of FeGa₃ above 300 K and a minimum in thermopower (−350 μV/K at 300 K) [348]. Hot press synthesis of Co-doped FeGa₃ leads to a *n*-type material with $zT = 0.21$ at 680 K [349]. RuGa₃ is also a small gap semiconductor, with 300 K large negative thermopower, and a maximum $zT = 0.18$ at 940 K [346].

RuGa₂ is another narrowband-gap semiconductor. Ga_{67−*x*}Ru_{33+*x*} samples prepared by a combination of arc-melting and SPS were show a maximum $zT = 0.50$ at 773 K for Ga_{66.6}Ru_{33.4} [350]. Ir substitution for Ru on RuGa₂ do not significantly improve TE properties, a maximum $zT = 0.31$ at 573 K being observed in Ir_{3.0}Ru_{30.4}Ga_{66.6} [351].

III–V compounds with the zinc blende structure have good power factors due to their high carrier mobility. In GaSb, Zn-doping slightly improves zT to 0.23 at 873 K [352], but the thermal conductivity is still very high, which opens the possibility of zT enhancement by reducing it. A successful thermal conductivity decrease has been obtained in the undoped material by nanostructuring, substituting Te for Sb and generating vacancies at the Ga site, but the high electrical resistivity prevented large zT values [353].

Initial report on CaZn₂Sb₂ with high electrical conductivity, comparable to β-Zn₄Sb₃, and a $zT = 0.52$ at 773 K [354] drives interest in the 122 composition. BaMn₂Sb₂ is a poor *n*-type TE [355], but in the Zintl phase Zn-doped YbZn_{2−*x*}Mn_{*x*}Sb₂ has a zT higher than 0.6 at 725 K [356]. The highest zT values have been reported in Yb_{1−*x*}Ca_{*x*}Cd₂Sb₂ (0.96 at 650 K) [357] and in YbCd_{2−*x*}Zn_{*x*}Sb₂ ($zT = 1.2$ at 700 K) [358].

Polycrystalline LnMg₂Bi₂ (Ln = Ca, Eu, Yb) are *p*-type materials with a high mobility but low carrier density that leads to relatively low zT (0.4 at 625 K with Yb) [359]. The role of minority carriers and defects, responsible for the extrinsic carriers, has been pointed out.

Recent zT first-principles predictions for organic materials pointed them as potential excellent TEs [360]. However, due to their decomposition at high temperatures, organic-based TEs are limited to applications near room temperature.

Conducting polymers might be capable of meeting the TE material characteristics and high PF have been known for a long time in the unstable and difficult to process iodine-doped polyacetylene [361]. The accurate control of the oxidation level in poly(3,4-ethylenedioxythiophene) (PEDOT), combined with its low intrinsic thermal conductivity, yields a $zT = 0.25$ at 300 K [362]. Low thermal conductivities and electrical resistivities, and reasonable Seebeck coefficients were reported for *n*-type poly[Na*x*(Ni-ett)], *n*-type poly[K*x*(Ni-ett)] and *p*-type poly[Cu*x*(Cu-ett)], with zT values of 0.1–0.2 at 400 K [363]. With the optimization of poly(styrenesulphonate) doping in poly(3,4-ethylenedioxythiophene) a very high zT of 0.42 has been recently achieved at 300 K [364].

In the case of composites made from polymers and high zT inorganic materials, the contact resistance between them is generally the limiting factor for further thermoelectric property improvement.

Several reviews on recent progress on organic-based TEs have been already published [15,365–367].

Quasicrystals (QC), with their very peculiar properties, seem to meet the requirements of a good TE material: low thermal conductivity, and high electrical conductivity and thermopower. Preliminary examination of Al-Pd-Mn properties ($zT \sim 0.1$ –0.2) leads to the initial proposition of studying QC for TE potential applications [368]. A $zT \sim 0.1$ at 600–700 K has been found in AlPdRe, but, interestingly, it is strongly dependent of the composition [369]. Replacing Al by Ga increases zT from 0.18 in Al₇₁Pd₂₀Mn₉ to 0.26 in Al₆₈Ga₃Pd₂₀Mn₉ [370].

A different approach from the one conventionally used during the last ten years and which consists in reducing subsequently the thermal conductivity from existing materials with high PF, is to start from materials with very poor thermal conductivity, characteristic of chalcogenide glasses, and try to improve their transport properties through addition of metallic elements (Cu, Ag, etc.) and the creation of nano-crystals inside the glass (glass-ceramics).

Initial proposition came from [371] and conducting glass in the Cu-Ge-Te system leads to small but promising $zT \sim 0.2$ at 300 K [372] (Fig. 16).

Melt spinning on Cu-As-Te system leads to a PF twice of that in Cu-Ge-Te, but no zT improvement was observed due to its higher thermal conductivity [373].

Varying the conditions of the SPS process enables the synthesis of composite glassy-crystalline Cu₁₅As₃₀Te₅₅ samples with different crystal/glass ratios (due to the partial crystallization of the amorphous matrix), leads to complex structure, and is an efficient tool to tune the electrical resistivity over several orders of magnitude, while maintaining low thermal conductivity values [374].

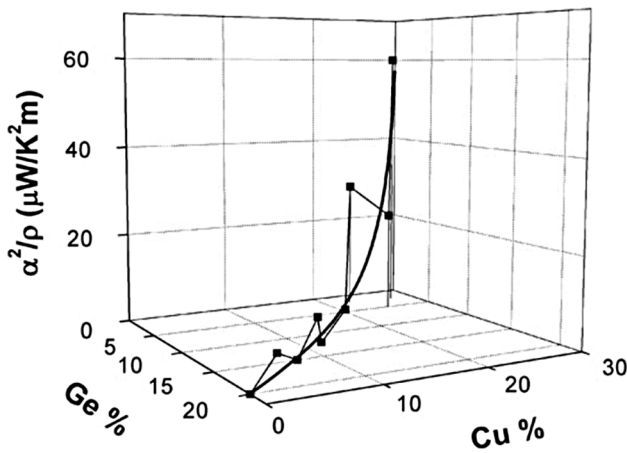


Fig. 16. Variation in the room temperature PF of $\text{Cu}_{x+y}\text{Ge}_{20-x}\text{Te}_{80-y}$ glasses as a function of composition [372].

3.6 Low temperature thermoelectrics

Most of the recent work on the development of thermoelectric materials has been devoted to room temperature and high temperature applications. However, albeit in less extension, the search of effective thermoelectric materials to be used on Peltier coolers to attend low and cryogenic temperatures has also been done.

Research has been mainly made on strongly correlated electron systems (SCES), particularly on Kondo insulators, as strong electron correlations frequently result in large values of Seebeck coefficient. The hybridization of localized d or f states with the conduction electron states may lead to the formation of a narrow (pseudo-) gap at low temperatures and a huge resonant density of states at the Fermi level can appear. As the Seebeck coefficient is function of the density of states slope near the Fermi level, large thermopower can emerge. The big Seebeck coefficient, conjugated with the relatively high electrical conductivity, lead to high PF at low temperatures. Good examples are the intermediate valence compounds CePd_3 and YbAl_3 , which have Seebeck coefficients of 100–120 $\mu\text{V}/\text{K}$ ($T \sim 150$ K) [375] and 80–90 $\mu\text{V}/\text{K}$ ($T \sim 250$ K) [376], respectively. Other SCES are $3d$ semiconductors like FeSi [377], FeGa_3 [348] and FeSb_2 [378], with Seebeck coefficients >500 $\mu\text{V}/\text{K}$ at 10–50 K. A short review of the thermoelectric power of correlated compounds was written by Oeschler et al. [379]. Although presenting large power factors, these materials also have high thermal conductivities (mainly due to the lattice contribution) and, consequently, small figures of merit. Attempts to decrease the thermal conductivity of known materials or to discover better ones have been recently reported.

Both CePd_3 and YbAl_3 crystallize in the cage like cubic AuCu_3 -type structure, where an octahedral empty space in the $1b$ position exists. Their thermal conductivity was successfully decreased by introducing B atoms [380,381], but better zT values were only obtained for YbAl_3 ($zT = 0.33$ at $T = 323$ K), as a degradation of the electrical transport properties of CePd_3 was observed. Recently, the introduction of other interstitial

atoms in the CePd_3 structure has been attempted, but no significant increase of zT was obtained [382]. Again, better performance on $\text{YbAl}_3 + \text{Mn}$ was obtained, the Mn doping lowering the lattice thermal conductivity without substantially affecting the PF and, consequently, increasing the figure of merit, to $zT = 0.4$ at ~ 300 K [383]. Alloying of CePd_3 , either in the Ce and Pd sites, was also tried [384–386], which resulted for CePd_2Pt in an increase to $zT = 0.3$ at $T = 250$ K [385], the highest value ever reported for any CePd_3 -based material at low temperatures. The partial substitution of Yb in YbAl_3 by other rare earths resulted in better materials, with a zT increase of $\sim 30\%$ at 250 K [387,388]. The thermoelectric properties of the Kondo lattice system $\text{Ce}(\text{Ni}_{1-x}\text{Cu}_x)_2\text{Al}_3$ were also investigated, the optimization of the composition leading to a maximum $zT = 0.125$ ($T = 100$ K) [389], which is comparable to values previously obtained in Kondo systems like $\text{Nd}_x\text{Ce}_{3-x}\text{Pt}_3\text{Sb}_4$ [390].

A large effort has been made to decrease the thermal conductivity of the FeSb_2 strongly correlated semiconductor, as its colossal power factor at low temperatures (~ 2300 $\mu\text{W K}^{-2} \text{cm}^{-1}$ at 12 K [391]) has made it a highly promising low temperature thermoelectric material. The effect of different chemical substitutions at the Fe and Sb sites has been investigated [378,392–394], being observed a decrease of the thermal conductivity with alloying. However, the decrease was not enough and/or the electrical properties were affected and no high zT values were achieved (a maximum $zT = 0.05$ at $T = 100$ K was observed for $\text{Fe}(\text{Sb}_{0.9}\text{Te}_{0.1})_2$ [394]). The decrease of the grain size leads to a drastic reduction of the thermal conductivity, but the Seebeck coefficient is also strongly degraded at low temperatures [395–397] and no significant zT improvement was obtained. The origin of the colossal Seebeck coefficient in FeSb_2 is still controversial, with some authors defending strong electron-electron correlations as the cause [391,392,398] and others suggesting as being due to the phonon drag effect [397,399,400].

Various transition-metal dopants on $\text{Fe}_{1-x}\text{M}_x\text{Si}$ alloys ($\text{M} = \text{Co}, \text{Ir}, \text{Os}$) improved zT from 0.007 at 60 K for pure FeSi to $zT = 0.08$ at 100 K for 4% Ir doping. The grain size decrease, on $\text{Fe}_{0.96}\text{M}_{0.04}\text{Si}$ alloys, reduces the thermal conductivity and zT became 0.125 at 100 K [401].

A new promising thermoelectric material for low-temperature applications, CsBi_4Te_6 , has been reported [402,403]. N - and p -type behavior can be achieved by doping and a maximum zT of 0.8 at 225 K was obtained. This value is much higher than those obtained for $\text{Bi}_{85}\text{Sb}_{15}$ -based solid solutions, where zT values of 0.33–0.10 at 120–210 K have been found [98,101,104]. Solid solutions of CsBi_4Te_6 with Sb and Se, with general formulas $\text{CsBi}_{4x}\text{Sb}_x\text{Te}_6$ and $\text{CsBi}_4\text{Te}_{6y}\text{Se}_y$ were recently synthesized and were also considered as potential TE materials [404], but the optimization of the composition and/or doping is still needed to obtain good properties.

Oxides have recently emerged as potential materials for low temperature thermoelectric cooling. The low temperature thermoelectric properties of LaFeAsO_{1-y} and $\text{LaFeAsO}_{1-x}\text{F}_x$ have been studied, and $zT = 0.06$ at

$T = 125$ K and $zT = 0.08$ at $T = 110$ K, respectively, have been determined [309,405]. A $\text{SrTi}_{0.99}\text{Nb}_{0.01}\text{O}_3$ perovskite single crystal was reported as having $zT = 0.07$ at $T = 40$ K [406], which is one of the largest among those previously reported below 50 K.

4 Shaping techniques for thermoelectrics

Apart from low-dimensional structures, such as thin films or nanowires, which can be used mainly in micro-systems, high zT thermoelectric (TE) nano-materials, made bulk, offer much greater prospects as applications for more effective TE modules.

Various techniques are available to synthesize nanostructured powders (easily transform in bulk), such as rapid solidification [407], spraying [408], solution chemistry [409] and the high energy milling [410,411].

The simple technique of mechanical alloying (MA) can produce significant amounts of Si-Ge alloy, Bi_2Te_3 , skutterudites, clathrates etc., depending on the type of attrition mills, planetary swing (or vibrating) in periods of a few hours to a few hundred hours. The materials produced are often nanometric powders or amorphous, which can be a positive contribution to the TE by reducing the materials thermal conductivity. The technique is suitable for the inclusion of dopants, but may in turn induce various contaminations. Finally, getting out of thermodynamic equilibrium phases can also be positive (new phases, peritectic phases without long time annealing. . .). The technique of fast quenching, which produces amorphous glasses of very low thermal conductivity, has recently been proposed for glasses with TE properties [371].

The solid material is then obtained using various consolidation techniques, some being described below. Using modern techniques of fast sintering, such as spark plasma sintering (SPS) [342,412,413], it is possible to obtain bulk nanostructured materials from nanopowders without significant grain size growth, this by reducing the time and temperature required for densification. These two techniques, MA and SPS, are increasingly used for formatting TE nano-materials.

Different extrusion techniques were used on TE materials, mainly on Bi_2Te_3 -derived ones [414,415], oxide type $\text{Ca}_3\text{Co}_4\text{O}_9$ [273] and “misfits”, in order to emphasize the grain orientation and optimize both mechanical and TE properties. Many references can be found in review [416]. To our knowledge, the technique has not yet been used on pre-sintered nano-powders, with preservation of a nano-structure.

The fast quenching (FQ) is a technique which leads to nanograined, glasses or amorphous. Chalcogenide glasses in the Cu-Ge-Te system, which are small gap semiconductors [372,417], and amorphous chalcogenides $\text{Ge}_{20}\text{Te}_{80-x}\text{Se}_x$ [418] have recently been studied for their potential TE.

In Na-doped AgSbTe_2 samples, melt quench + SPS improves zT to 1.5 (570 K). The TE performance of melt spinning (MS) + SPS AgSbTe_2 samples with nanopores improves even more, and a zT of 1.65 is achieved at 570 K,

which increases 35% and 200% when compared with samples prepared by melt-quench-SPS and traditional melting and slow-cooling methods [163,166].

FQ of layered compounds from the Ge-Sb-Te system, followed by hot pressing, has increased the PF in the nanostructured materials [419], the FQ technique being of general interest in TE.

MS and SPS of $\text{MnSi}_{1.75}$ materials increases zT to 0.62 at 600 K by in-situ forming nano-phase of MnSi [80].

$\text{In}_4(\text{Se}_{1-x}\text{Te}_x)_3$ synthesized by melt quenching and SPS post treatment show that the Te substitution reduces the thermal conductivity, In_4Te_3 having the lowest one [224].

MS and SPS were used to prepare high-performance *p*-type Bi_2Te_3 materials with layered nanostructure, the electrical conductivity increasing and thermal conductivity decreasing with the increase of the linear speed, which leads to a maximum $zT = 1.35$ at 300 K [420].

$\text{Bi}_{85}\text{Sb}_{15}$ alloys were prepared by MS and subsequent SPS, and increasing the cooling rate in the MS process optimizes the PF and reduces the thermal conductivity, leading to a zT of 0.99 at 700 K [98].

The addition of a uniaxial pressure, pressure sintering, promotes welding of grains but also the orientation of the powder particles, especially if no lateral blocking limits the lateral deformation of the assembly. This proves interesting for TE anisotropic materials in order to promote best conductors plans (electric) than others. The reached density should be the highest possible ($\geq 95\%$) to avoid an increase in the electrical resistivity intergranular effect. However, in many systems of hot uniaxial press (HUP) the powdered material is initially contained in a crucible and the side effects of the crucible edge on the orientation are not negligible. The comparison with the hot isotropic pressing (HIP) performed on the Si-Ge system TE (*p*-doped or GaP) proved inconclusive [421] and experimental constraints and cost of HIP make that the TE materials are rather treated by HUP. When certain elements are volatile, as in PbS or PbSe, it is possible to use the HIP with sealed capsules [422].

The HUP was used to compact nanopowders of various TE materials fabricated by different methods, with good final zT values.

Thallium doped PbTe samples, prepared either by melting, slow cooling, long time annealing, post-crushing and hot pressing or by MA and hot pressing, show a high $zT = 1.3$ at 673 K [423,424].

By MA alloying $\text{Bi}_x\text{Sb}_{2-x}\text{Te}_3$ bulk crystalline ingots or Bi, Sb and Te elemental chunks, followed by hot pressing, high $zT = 1.3$ were obtained at ~ 700 K [425,426].

MA and hot press lead to $zT = 0.2$ at 600 K in CrSi_2 , despite the Fe contamination due to MA [92].

In Mg_3Sb_2 derivatives, zT stays very low (0.01) in $(\text{Mg}_{0.7}\text{Cd}_{0.25}\text{Ag}_{0.05})_3\text{Sb}_2$ [427], but the zT of $(\text{Mg}_{1-x}\text{Zn}_x)_3\text{Sb}_2$ with $x = 0.32$ has been found to be over 80 times larger than that of Mg_3Sb_2 at 300 K [113]. In order to improve zT of Mg_2Si derivatives, MA and hot pressing of $\text{Mg}_2\text{Si}_n\text{Sn}_{1-n}$ has been tried and values as high as 0.9 at 773 K were obtained [428].

Polycrystalline samples of composition $\text{Ga}_{1+x}\text{Ge}_{1-x}\text{Te}$ ($x = -0.03$ to 0.07) and GaGeTe_{1-y} ($y = -0.02$ to 0.02) prepared by hot pressing are p -type materials, but with low PF [429].

By MA and hot press a zT of 0.28 at 820 K has been reached in $\text{MnSi}_{1.73}$ [86].

High zT values were also obtained in TAGS: $zT = 1.75$ (773 K) in TAGS80, $zT = 1.4$ (773 K) in TAGS85 and $zT = 1.6$ (773 K) in Bi_2Te_3 doped $\text{Ge}_{0.87}\text{Pb}_{0.13}\text{Te}$ [184].

High zT values (>1) at high temperature (>1200 K) can be obtained in n - and p -type Si-Ge alloys with the help of nanostructuring, the decreasing of Ge content lowering their cost [430,431].

Shaping by HUP significant amount of LAST ingots can be used for producing modules [432].

Since the 2000s, the densification of thermoelectric materials often uses techniques under pressure sintering assisted by electric current (ECAS “Electric Current Assisted (Activated) Sintering”), various names can be found depending on specific characteristics. In the case of pulsed current, the name of SPS “Spark Plasma Sintering” becomes popular, although probably without “plasma” [433]. The time savings (temperature rises to ~ 1000 °C/min) for an equivalent densification to that obtained by HUP ($>95\%$, essential in TE), is also advantageous from an economic point of view and easily transferable to an industrial scale. This fast process limits the time available for grain growth and thus make easier to obtain nano-structured materials “perfectly” densified. A comprehensive review on the subject ECAS was completed in 2009 [434].

Note that, in the one hand, some unconventional TE materials, such as SiB_6 , can be densified by SPS (unlike the HUP), and, in the other, although the current “must” cross the sample, sintering oxides (even Al_2O_3) is possible, as the initial heating of the graphite crucible leads to an increase of the sample temperature and a more conductive oxide. The manufacture of semiconducting TE materials is often done by hot pressing techniques [435] because the doping levels of TE are often strong enough and the properties are not too affected by contamination induced by powder technology (induced at the MA or graphite at the SPS).

In the case of TE nano-materials and nano-composites it is obviously that SPS has a distinct advantage within the maintenance of a nanostructure. This point is well illustrated by the sintering of CoSb_3 nano-powders (prepared by solvothermal method (S)) by hot pressure (HP) at 823 K under 50 MPa in 30 min and by SPS at 853 K under 40 MPa in 5 min, and by compare them to the material obtained by melting and HP (M-HP). Although the densities obtained are not very high ($<94\%$) the best zT is obtained for the SPS material (Fig. 17), probably because its final grain size of 150 nm instead of 250 for the HP material.

Surprisingly, one of the first articles on the use of SPS on TE nanomaterials concerns a difficult case to make: the functionally graded materials from powders prepared by MA of $\text{Mg}_2\text{Si} + \text{FeSi}_2$ consolidated by SPS [413].

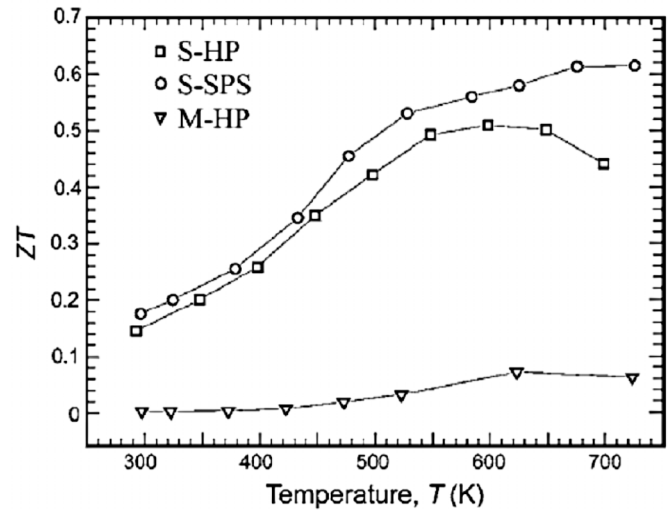


Fig. 17. Figure of merit CoSb_3 (T) sintered under various conditions (Ref. [436]).

The discovery of a $zT > 2$ in the n -type $\text{Ag}_n\text{Pb}_m\text{SbTe}_{m+2n}$ (LAST- m) has attracted the interest of its simplified preparation by MA + SPS. However prepared material is then p -type (Pb loss?) and has lower zT (<1.4 at 673 K) [191]. Annealing for 30 days enhances zT (1.5 to 700 K) [192]. The study of sintering SSP (sintering in solid phase), HIP and SPS lead to a Seebeck coefficient inhomogeneous in the HIP phase [437] (Fig. 18).

Substitution $\text{Te} \rightarrow \text{Se}$ in nanopowders (~ 35 nm) of $\text{AgPb}_m\text{SbSe}_{m+2}$ (LASS- m , $m = 10, 12, 16, 18$), $\text{Ag}_x\text{Pb}_{18}\text{SbSe}_{20}$ ($x = 0.8, 0.85$) and $\text{AgPb}_{18}\text{SbSe}_{20-y}\text{Te}_y$ ($y = 1, 3$), sintered either by SSP or SPS, leads to p -type materials having a microstructure or nano/micro mixture (composite), respectively [438].

Bulk $\text{AgPb}_x\text{SbTe}_{20}$ ($x = 20, 21$ and 22.5) compounds were fabricated by the combination of melting, milling and SPS, and the same compositional bulk samples were fabricated by MA-SPS for comparison. Both methods lead to zT in the range 0.9–1.2 at 725 K with a maximum in $\text{AgPb}_{20}\text{SbTe}_{20}$ [193]. MA-SPS method is then advantageous because of the simplicity of MA as a low-temperature process.

Nanostructuring the well-known B-doped Si-Ge TE material and densifying using a hot press with DC current increases the value of zT , in p -type, to 0.95 at ~ 1050 K. This value, in a material that has local characteristics of a nanocomposite, offers 50% improvement over the best p -material [439].

In many cases, the consolidation by SPS concerns nanocomposites of various materials with improved PF and/or zT .

The insertion of micro-grains of Bi with Fe_2VAl nanoparticles facilitates densification of the composite (Bi liquid) during SPS sintering and reduces the resistivity, in addition to the thermal conductivity, of the composite $\text{Fe}_2\text{VAl}_{0.9}\text{Si}_{0.1}/\text{Bi}$ and zT increases [440]. The dominant effect on the thermal conductivity also slightly improves zT of the $\text{Fe}_2\text{VAl}_{0.9}\text{Si}_{0.1}$ Heusler alloy [441].

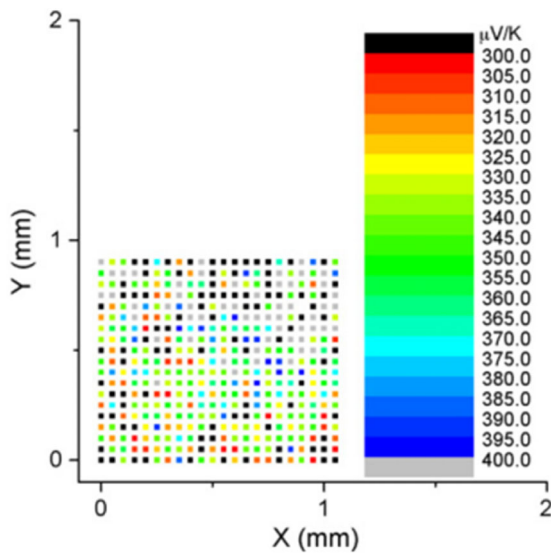


Fig. 18. Room temperature Seebeck coefficient scanning image of the polished surface of LAST-10 sample [437].

The same effect on TE properties of mixing grain size (known in skutterudites) at constant chemical composition was observed in PbTe [442,443] and Bi₂Te₃ [444].

N-type composites of PbTe and PbS with Bi-doping in Pb_{0.999}Te_{0.88}Sb_{0.12}Bi_{0.001} prepared by MA and SPS leads to a zT of 1.2 at 570 K [445], the same zT value being obtained in Pb_{0.996}Te_{0.88}Sb_{0.12}Sb_{0.004} by Sb doping, but at 770 K [446].

A zT of 0.74 in Sb₂Te₃ has been increased to 0.84 by Ge doping and SPS treatment in Sb₁₀₀GeTe₁₅₀ [233].

Higher manganese silicides MnSi_{*x*}, made of non-toxic and abundant elements, could replace PbTe for TE applications in middle-high temperatures (~800 K), as after SPS handling zT values approaches 0.7 [83,85].

Al-Mg₂Si processed by MA and SPS leads to a zT of 0.5 at 800 K [57]. In the same way, Sn-Sb [447] does not improve the zT of 1.1 reported for Mg₂Si_{1-*x*}Sn_{*x*} [61].

In Mg₂Si composites with Al₂O₃, Bi₂O₃, or Sb₂O₃, zT were found to be also smaller, 0.58, 0.68, and 0.63 at 865 K, respectively [58].

The previous examples show that the pressure sintering has led to an improvement of the characteristics of the vast majority of TE materials, when nano-structured. This seems to be even more efficient when two TE materials are used to make a nano-composite [180]. With the same CoSb₃ skutterudite, the TE properties are improved if there is no chemical reaction with ZnO [448], with CeO₂ [449] or if there is no substitution of Sb for Te on PbTe/CoSb₃ composites [450].

HIP has been used to make the branches (*p* and *n*) of a module based on Si-Ge with their electrodes [451].

Although the technique for making contacts on nanowires was studied [452,453], techniques of sintering under pressure are more likely to be applied to massive nano-structured samples, not only for the shaping but also to achieve contact.

A set powder CoSb₃/Ti leaf inserted/Mo-Cu electrode can be assembled in a single operation by SPS, forming a good electrical contact [454]. During accelerated aging tests, intermetallic layers CoSb₃/TiCoSb/TiSb₂/TiSb/Ti form, whose evolution lead to a period of several years for operation of CoSb₃ at 500 °C [455]. The W-Cu electrode (one step SPS process) has good stability at high temperatures [454,456].

The microwave sintering is well-established and is increasingly used for the treatment of materials. The specificity of this heating technique is characterized, as the SPS method, by very short treatment times, typically of the order of a few minutes. The microwave sintering can also lead to specific microstructures, which can be useful for TE materials. This technique starts to be used for different TE systems: skutterudites [457], PbTe and Bi₂Te₃ [458]. A comparative study on one batch of Bi₂Te₃ nanopowder treated by microwave sintering, HIP and SPS has recently appeared, and best zT for the studied composition being obtained with microwave and SPS (0.75) [459].

5 Summary

Significant advances to improve the transport properties of bulk TE materials have been made in the last years. The adoption of new strategies, in particular those based on the “phonon glass and electron crystal”, PGEC, concept, led to the discovery of novel materials with figures of merit as high as 2, in particular based on the classical Bi₂Te₃ and PbTe materials. However, their use with mass production depends not only on the materials TE efficiency, but also on other aspects, as cost, availability, environmental, etc. The study of materials other than the TE classical ones is therefore essential. Herein, an overview of the actual knowledge on the new potential TE bulk materials based on intermetallics, pnictides and chalcogenides was given. Albeit not being exhaustive (the number of published articles on TE per year is approaching 1000), the most promising of these bulk systems were reviewed, with special emphasis on silicides, antimonides, tellurides, sulfides and selenides. Due to its importance for applications and development of new materials, many of them based on nano-structured material, a brief description of the shaping techniques for thermoelectrics was also given.

The authors would like to thank the French National Agency (ANR) in the frame of its programme “PROGELEC” (Verre Thermo-Générateur “VTG”).

Glossary

COP: coefficient of performance

C_p : specific heat per unit volume

e^- : electron

\vec{E} : electric field

ECAS: electric current assisted (activated) sintering

FQ: fast quenching

h^+ : hole
 HIP: hot isotropic pressing
 HMS: higher manganese silicides
 HP: hot pressure
 HUP: hot uniaxial press
 I : electric current
 \vec{j} : electric current density
 l : mean free path of phonons
 L : Lorentz number
 LAST: $(\text{PbTe})_x-(\text{AgSbTe}_2)_{1-x}$ materials
 LASTT: $\text{Ag}(\text{Pb}_{1-x}\text{Sn}_x)_m\text{SbTe}_{2+m}$ materials
 MA: mechanical alloying
 MS: melt spinning
 n : carrier concentration
 PAS: plasma assisted sintering
 PF: power factor
 PGEC: phonon glass and electron crystal
 q : charge of a carrier
 \vec{q} : heat flow
 Q : heat quantity
 S: solvothermal method
 S_a : transport entropy per charge carrier
 SALT: $\text{Na}_{1-x}\text{Pb}_m\text{Sb}_y\text{Te}_{m+2}$ materials
 SCES: strongly correlated electron systems
 SPS: Spark plasma sintering
 SSP: sintering in solid phase
 T : absolute temperature
 T_h : hot temperature
 T_c : cold temperature
 TAGS: silver antimony germanium telluride alloys
 TE: thermoelectric
 zT : figure of merit of a material
 ZT : figure of merit of a thermoelectric couple
 α : Seebeck coefficient
 α_{ab} : Seebeck coefficient of a two materials (a and b) circuit
 ΔT : temperature difference
 ΔV : electrical potential difference
 $\vec{\nabla}T$: temperature gradient
 η_{\max} : maximum conversion efficiency for electricity generation
 λ : thermal conductivity
 λ_e : electronic contribution to the thermal conductivity
 λ_L : lattice (phonon) contribution to the thermal conductivity
 μ_q : mobility
 Π : Peltier coefficient
 Π_{ab} : Peltier coefficient of a two materials (a and b) circuit
 ρ : electrical resistivity
 σ : electrical conductivity
 $\sigma\alpha^2$: power factor
 τ : Thomson coefficient
 ν : speed of sound

References

- R. Saidur, M. Rezaei, W.K. Muzammil, M.H. Hassan, S. Paria, M. Hasanuzzaman, *Renew. Sust. Energy Rev.* **16**, 5649 (2012)
- A.P. Gonçalves, C. Godart, in *New Materials for Thermoelectric Applications: Theory and Experiment*, NATO ASI Series B edited by V. Zlatić, A. Hewson (Springer, 2013), pp. 1–24
- A. Weidenkaff, L. Bocher, R. Robert, M. Aguirre, D. Logvinovich, *Mater. Res. Soc. Symp. Proc.* **1044**, U07 (2008)
- S. Hebert, A. Maignan, in *Functional Oxides* edited by D.W. Bruce, D. O'Hare, R.I. Walton (John Wiley & Sons, Ltd, Chichester, 2010)
- K. Koumoto, R. Funahashi, E. Guilmeau, Y. Miyazaki, A. Weidenkaff, Y. Wang, C. Wan, *J. Am. Ceram. Soc.* **96**, 1 (2013)
- H. Itahara, T. Tani, *R&D Review of Toyota CRDL* **39**, 63 (2004)
- D. Bérardan, E. Guilmeau, A. Maignan, B. Raveau, *Solid State Commun.* **146**, 97 (2008)
- W.M. Kim, F.D. Rosi, *Solid State Electron.* **15**, 1121 (1972)
- L.D. Hicks, M.S. Dresselhaus, *Phys. Rev. B* **47**, 12727 (1993)
- H.J. Goldsmid, in *Proceedings 23rd International Conference on Thermoelectrics, Adelaide, Australia, 25–29 July 2004*
- G.S. Nolas, S.J. Poon, M.G. Kanatzidis, *MRS Bull.* **31**, 199 (2006)
- J.R. Sootsman, D.Y. Chung, M.G. Kanatzidis, *Angew. Chem. Int. Ed. Engl.* **48**, 8616 (2009)
- A.J. Minnich, M.S. Dresselhaus, Z.F. Ren, G. Chen, *Energy Environ. Sci.* **2**, 466 (2009)
- W. Liu, X. Yan, G. Chen, Z. Ren, *Nano Energy* **1**, 42 (2012)
- M. Martín-González, O. Caballero-Calero, P. Díaz-Chao, *Renew. Sust. Energy Rev.* **24**, 288 (2013)
- H. Alama, S. Ramakrishna, *Nano Energy* **2**, 190 (2013)
- J. Kimmel, *Thermoelectric Materials Physics* **152**, Special Topics Paper (1999)
- Z.H. Dughaish, *Physica B* **322**, 205 (2002)
- M.S. Dresselhaus, G. Chen, M.Y. Tang, R. Yang, H. Lee, D. Wang, Z. Ren, J.P. Fleurial, P. Gogna, *Adv. Mater.* **19**, 1043 (2007)
- M.S. El-Genk, H.H. Saber, T. Caillat, *Energy Conversion and Management* **44**, 1755 (2003)
- H.J. Goldsmid, G.S. Nolas, in *Proceedings 20th International Conference on Thermoelectrics, 8–11 June, Beijing, China, 2001*, p. 1
- J.P. Fleurial, T. Caillat, A. Borshchevsky, in *Proceedings 14th International Conference on Thermoelectrics, 1995*, pp. 231–235
- A. Borshchevsky, T. Caillat, J.P. Fleurial, in *Proceedings 15th International Conference on Thermoelectrics, 26–29 March, Pasadena, CA, USA, 1996*, p. 112
- T. Caillat, J.P. Fleurial, A. Borshchevsky, in *Proceedings 15th International Conference on Thermoelectrics, March, Pasadena, CA, USA, 1996*, p. 100
- C. Uher, *Semiconductors and semi metals* (Academic Press, San Diego, 2001), p. 119

26. L. Chen, in *Proceedings 21st International Conference on Thermoelectrics, Long Beach, California, USA, August 25–29, 2002*, p. 42
27. S. Bühler-Paschen, C. Godart, Y.N. Grin, in *Complex Metallic Alloys, Fundamental and Applications*, edited by J.-M. Dubois, E. Belin-Ferré (Wiley-VCH Verlag GmbH & Co. KGaA, Weinheim, 2011), Chap. 9, pp. 365–384
28. P. Rogl, Y. Mudryk, C. Paul, S. Berger, E. Bauer, G. Hilscher, C. Godart, H. Noël, in *Proceedings 22nd International Conference on Thermoelectrics ICT2003, La Grand Motte, France, August, 2003*
29. H. Kleinke, *Chem. Mater.* **22**, 604 (2010)
30. C. Godart, A.P. Gonçalves, E.B. Lopes, B. Villeroy, in *Properties and Applications of Thermoelectric Materials*, NATO ASI Series B edited by V. Zlatic (Springer, 2009), pp. 19–49
31. T.J. Seebeck, *Abh. Akad. Wiss. Berlin* **1820–1821**, 289 (1822)
32. J.C. Peltier, *Ann. Chim. (Paris)* **1**, 371 (1834)
33. W. Thomson, *Proc. R. Soc. Ed.* 91 (1851)
34. G.D. Mahan, B.C. Sales, J. Sharp, *Phys. Today* **50**, 42 (1997)
35. G.S. Nolas, J. Sharp, H.J. Goldsmid, *Thermoelectrics: Basic principles and New Materials developments*, Springer Series (Springer-Verlag, 2001), Vol. 45
36. G.A. Slack, in *Thermoelectric Handbook*, edited by D.M. Rowe (CRC press, Boca Raton, FL, 1995), p. 407
37. B. Abeles, *Phys. Rev.* **131**, 1906 (1963)
38. J. Callaway, H.C. von Baeyer, *Phys. Rev.* **120**, 1149 (1960)
39. P.G. Klemens, *Phys. Rev.* **119**, 507 (1960)
40. J.M. Worlock, *Phys. Rev.* **147**, 636 (1966)
41. G.S. Nolas, H.J. Goldsmid, *Phys. Stat. Sol. A* **194**, 271 (2002)
42. *Thermoelectrics Handbook: Macro to Nano*, edited by D.M. Rowe (CRC Taylor & Francis, Boca Raton, 2006)
43. C. Godart, A.P. Gonçalves, E.B. Lopes, B. Villeroy, *Spring meeting MRS 2009, San Francisco, USA, April 13–17*, Vol. 1166-N08-01, pp. 183–193
44. Y. Gelbstein, J. Davidow, S.N. Girard, D.Y. Chung, M. Kanatzidis, *Adv. Energy Mater.* **3**, 815 (2013)
45. E.N. Nikitin, *Zhur. Tekhn. Fiz.* **28**, 23 (1958)
46. C.B. Vining, *Thermoelectric Properties of Silicides*, in *Thermoelectric Handbook* edited by D.M. Rowe (CRC press, Boca Raton, FL, 1995)
47. M.I. Fedorov, V.K. Zaitsev, *Thermoelectrics of Transition Metal Silicides*, in *Thermoelectric Handbook* edited by D.M. Rowe (CRC press, Boca Raton, FL), Vol. 31
48. M.I. Fedorov, *J. Thermoelectr.* **2**, 51 (2009)
49. J. Tani, G. Kido, *Physica B* **364**, 218 (2005)
50. S.-M. Choi, K.-H. Kim, I.-H. Kim, S.-U. Kim, W.-S. Seo, *Curr. Appl. Phys.* **11**, S388 (2011)
51. S. Fiameni, S. Battiston, S. Boldrini, A. Famengo, F. Agresti, S. Barison, M. Fabrizio, *J. Solid State Chem.* **193**, 142 (2012)
52. M. Akasaka, T. Iida, A. Matsumoto, K. Yamanaka, Y. Takanashi, T. Imai, N. Hamada, *J. Appl. Phys.* **104**, 013703 (2008)
53. J.I. Tani, H. Kido, *Jpn J. Appl. Phys.* **46**, 3309 (2007)
54. J.I. Tani, H. Kido, *Intermetallics* **15**, 1202 (2007)
55. T. Dasgupta, C. Stiewe, R. Hassdorf, A.J. Zhou, L. Boettcher, E. Müller, *Phys. Rev. B* **83**, 235207 (2011)
56. M. Ioannou, G. Polymeris, E. Hatzikraniotis, A.U. Khan, K.M. Paraskevopoulos, T. Kyratsi, *J. Electron. Mater.* **42**, 1827 (2013)
57. S. Battiston, S. Fiameni, M. Saleemi, S. Boldrini, A. Famengo, F. Agresti, M. Stingaciu, M.S. Toprak, M. Fabrizio, S. Barison, *J. Electron. Mater.* **42**, 1956 (2013)
58. J.I. Tani, H. Kido, *Intermetallics* **32**, 72 (2013)
59. Q.S. Meng, W.H. Fan, R.X. Chen, Z.A. Munir, *J. Alloys Compd.* **509**, 7922 (2011)
60. Q. Zhang, X.B. Zhao, H. Yin, T.J. Zhu, *J. Alloys Compd.* **464**, 9 (2008)
61. V.K. Zaitsev, M.I. Fedorov, E.A. Gurieva, I.S. Eremin, P.P. Konstantinov, A.Y. Samunin, M.V. Vedernikov, *Phys. Rev. B* **74**, 045207 (2006)
62. M. Søndergaard, M. Christensen, K.A. Borup, H. Yin, B.B. Iversen, *J. Mater. Sci.* **48**, 2002 (2013)
63. S.-C. Zhou, C.-G. Bai, *J. Cent. South Univ.* **19**, 2421 (2012)
64. M.I. Fedorov, V.K. Zaitsev, M.V. Vedernikov, in *Proceedings 25th International Conference on Thermoelectrics, 6–10 August, Vienna, 2006*
65. J.J. Pulikkotil, D.J. Singh, S. Auluck, M. Saravanan, D.K. Misra, A. Dhar, R.C. Budhani, *Phys. Rev. B* **86**, 155204 (2012)
66. J.I. Tani, H. Kido, *J. Alloys Compd.* **466**, 335 (2008)
67. Z. Du, T. Zhu, X. Zhao, *Mater. Lett.* **66**, 76 (2012)
68. Z.L. Du, G.Y. Jiang, Y. Chen, H.L. Gao, T.J. Zhu, X.B. Zhao, *J. Electron. Mater.* **41**, 1222 (2012)
69. A.U. Khan, N. Vlachos, T. Kyratsi, *Scripta Mater.* **69**, 606 (2013)
70. H. Ihou-Mouko, C. Mercier, J. Tobola, G. Pont, H. Scherrer, *J. Alloys Compd.* **509**, 6503 (2011)
71. W. Liu, K. Yin, X. Su, H. Li, Y. Yan, X. Tang, C. Uher, *Intermetallics* **32**, 352 (2013)
72. G. Jiang, L. Chen, J. He, H. Gao, Z. Du, X. Zhao, T.M. Tritt, T. Zhu, *Intermetallics* **32**, 312 (2013)
73. S.W. Kim, Y. Mishima, D.C. Choi, *Intermetallics* **10**, 177 (2002)
74. Y.K. Kuo, K.M. Sivakumar, S.J. Huang, C.S. Lue, *J. Appl. Phys.* **98**, 123510 (2005)
75. H. Sun, X. Lu, D.T. Morelli, *J. Electron. Mater.* **42**, 1352 (2013)
76. B.A. Simkin, Y. Hayashi, H. Inui, *Intermetallics* **13**, 1225 (2005)
77. N.L. Okamoto, T. Koyama, K. Kishida, K. Tanaka, H. Inui, *Acta Mater.* **57**, 5036 (2009)
78. N.L. Okamoto, T. Koyama, K. Kishida, K. Tanaka, H. Inui, *J. Electron. Mater.* **39**, 1640 (2010)
79. A.J. Zhou, X.B. Zhao, T.J. Zhu, S.H. Yang, T. Dasgupta, C. Stiewe, R. Hassdorf, E. Mueller, *Mater. Chem. Phys.* **124**, 1001 (2010)
80. W. Luo, H. Li, Y. Yan, Z. Lin, X. Tang, Q. Zhang, C. Uher, *Intermetallics* **19**, 404 (2011)
81. W. Luo, H. Li, F. Fu, W. Hao, X. Tang, *J. Electron. Mater.* **40**, 1233 (2011)
82. Y. Sadia, Y. Gelbstein, *J. Electron. Mater.* **41**, 1504 (2012)
83. Y. Sadia, L. Dinnerman, Y. Gelbstein, *J. Electron. Mater.* **42**, 1926 (2013)
84. Z. Zamanipoura, X. Shi, M. Mozafari, J.S. Krasinski, L. Tayebi, D. Vashae, *Ceram. International* **39**, 2353 (2013)
85. A. Famengo, S. Battiston, M. Saleemi, S. Boldrini, S. Fiameni, F. Agresti, M.S. Toprak, S. Barison, M. Fabrizio, *J. Electron. Mater.* **42**, 2020 (2013)

86. D.K. Shin, K.W. Jang, S.C. Ur, I.-H. Kim, J. Electron. Mater. **42**, 1756 (2013)
87. C. Drasar, E. Mueller, A. Mrotzek, G. Karpinski, in *Proceedings of 21st ICT, Long Beach, California, USA, Aug. 25–29, 2002*, p. 81
88. M. Ito, H. Nagai, E. Oda, S. Katsuyama, K. Majima, J. Appl. Phys. **91**, 2138 (2002)
89. S.W. Kim, M.K. Cho, Y. Mishima, D.C. Choi, Intermetallics **11**, 399 (2003)
90. K.F. Cai, E. Mueller, C. Drasar, C. Stiewe, Solid State Commun. **131**, 325 (2004)
91. Z. He, D. Platzek, C. Stiewe, H. Chen, G. Karpinski, E. Müller, J. Alloys Compd. **438**, 303 (2007)
92. T. Dasgupta, A.M. Umarji, J. Alloys Compd. **461**, 292 (2008)
93. S. Perumal, S. Gorsse, U. Ail, B. Chevalier, R. Decourt, A.M. Umarji, J. Mater. Sci. **48**, 227 (2013)
94. G.E. Smith, R. Wolfe, J. Appl. Phys. **33**, 841 (1962)
95. B. Lenoir, M. Cassart, J.-P. Michenaud, H. Scherrer, S. Scherrer, J. Phys. Chem. Solids **57**, 89 (1996)
96. R. Martin-Lopez, B. Lenoir, A. Dauscher, X. Devaux, W. Diimmler, H. Scherrer, M. Zandona, J.F. Remy, Scripta Mater. **37**, 219 (1997)
97. B. Landschreiber, E. Günes, G. Homm, C. Will, P. Tomes, C. Rohner, A. Sesselmann, P.J. Klar, S. Paschen, E. Müller, S. Schlecht, J. Electron. Mater. **42**, 2356 (2013)
98. T. Luo, S. Wang, H. Li, X. Tang, Intermetallics **32**, 96 (2013)
99. C. Song, J. Feng, R. Huang, L. Li, Procedia Engineering **27**, 193 (2012)
100. K.C. Lukas, G. Joshi, K. Modic, Z.F. Ren, C.P. Opeil, J. Mater. Sci. **47**, 5729 (2012)
101. Y.S. Hor, R.J. Cava, J. Alloys Compd. **479**, 368 (2009)
102. Z. Chen, M. Zhou, R. Huang, C. Huang, C. Song, Y. Zhou, L. Li, J. Electron. Mater. **41**, 1725 (2012)
103. F. Samedov, M. Tagiev, Turk. J. Phys. **22**, 131 (1998)
104. Z. Chen, M. Zhou, R.J. Huang, C.M. Song, Y. Zhou, L.F. Li, J. Alloys Compd. **511**, 85 (2012)
105. R. Wolfe, G.E. Smith, Appl. Phys. Lett. **1**, 5 (1962)
106. W.M. Yim, A. Amith, Solid State Electronics **15**, 1141 (1972)
107. O. Yamashita, K. Satou, H. Odahara, S. Tomiyoshi, J. Appl. Phys. **98**, 073707 (2005)
108. A. Bentien, S. Johnsen, G.K.H. Madsen, B.B. Iversen, F. Steglich, Europhys. Lett. **80**, 17008 (2007)
109. H.J. Li, X.Y. Qin, D. Li, J. Alloys Compd. **467**, 299 (2009)
110. H.J. Li, X.Y. Qin, D. Li, H.X. Xin, J. Alloys Compd. **472**, 400 (2009)
111. T. Kajikawa, N. Kimura, T. Yokoyama, in *Proceedings 22nd ICT, La Grand Motte, France, August, 2003*, p. 305
112. C.L. Condrón, S.M. Kauzlarich, F. Gascoin, G.J. Snyder, J. Solid State Chem. **179**, 2252 (2006)
113. H.X. Xin, X.Y. Qin, J.H. Jia, C.J. Song, K.X. Zhang, J. Zhang, J. Phys. D **42**, 165403 (2009)
114. V. Ponnambalam, D.T. Morelli, J. Electron. Mater. **42**, 1307 (2013)
115. A. Bhardwaj, A. Rajput, A.K. Shukla, J.J. Pulikkotil, A.K. Srivastava, A. Dhar, G. Gupta, S. Auluck, D.K. Misra, R.C. Budhani, RSC Adv. **3**, 8504 (2013)
116. T. Caillat, J.P. Fleurial, A. Borshchevsky, in *15th International Conference on Thermoelectrics, 1996*, pp. 151–154
117. T. Caillat, J.P. Fleurial, A. Borshchevsky, J. Phys. Chem. Solids **58**, 1119 (1997)
118. T.J. Zhu, X.B. Zhao, M. Yan, S.H. Hu, S.H. Li, B.C. Zhou, Mater. Lett. **46**, 44 (2000)
119. S.C. Ur, P. Nash, I.H. Kim, J. Mater. Sci. **38**, 3553 (2003)
120. S.C. Ur, I.H. Kim, P. Nash, in *Proceedings of 22nd ICT, La Grand Motte, France, August, 2003*, p. 251
121. L.T. Zhang, M. Tsutsui, K. Ito, M. Yamaguchi, J. Alloys Compd. **358**, 252 (2003)
122. B.L. Pedersen, H. Birkedal, B.B. Iversen, M. Nygren, P.T. Frederiksen, Appl. Phys. Lett. **89**, 242108 (2006)
123. G. Nakamoto, N. Akai, M. Kurisu, J. Alloys Compd. **437**, 151 (2007)
124. G. Nakamoto, K. Kinoshita, M. Kurisu, J. Appl. Phys. **105**, 013713 (2009)
125. G.J. Snyder, M. Christensen, E. Nishibori, T. Caillat, B.B. Iversen, Nat. Mater. **3**, 458 (2004)
126. F. Cargnoni, E. Nishibori, P. Rabiller, L. Bertini, G.J. Snyder, M. Christensen, C. Gatti, B.B. Iversen, Chem. Eur. J. **10**, 3861 (2004)
127. B.L. Pedersen, H. Birkedal, E. Nishibori, A. Bentien, M. Sakata, M. Nygren, P.T. Frederiksen, B.B. Iversen, Chem. Mater. **19**, 6304 (2007)
128. W. Li, L. Zhou, Y. Li, J. Jiang, G. Xu, J. Alloys Compd. **486**, 335 (2010)
129. L. Pan, X.Y. Qin, M. Liu, F. Liu, J. Alloys Compd. **489**, 228 (2010)
130. F.S. Liu, L.C. Pan, W.Q. Ao, L.P. He, X.X. Li, H.T. Li, J.Q. Li, J. Electron. Mater. **41**, 2118 (2012)
131. T. Koyanagi, K. Hino, Y. Nagamoto, H. Yoshitake, K. Kishimoto, in *Proceedings of 16th International Conference on Thermoelectrics, Dresden, 1997*, p. 463.
132. L. Pan, X.Y. Qin, M. Liu, Solid State Commun. **150**, 346 (2010)
133. H.J. Gau, J.L. Yu, C.C. Wu, Y.K. Kuo, C.H. Ho, J. Alloys Compd. **480**, 73 (2009)
134. J.L. Cui, H. Fu, L.D. Mao, D.Y. Chen, X.L. Liu, J. Appl. Phys. **106**, 023702 (2009)
135. E. Dashjav, A. Szczepienowska, H. Kleinke, J. Mater. Chem. **12**, 345 (2002)
136. F. Gascoin, J. Rasmussen, G.J. Snyder, J. Alloys Compd. **427**, 324 (2007)
137. H. Xu, K.M. Kleinke, T. Holgate, D. Rossouw, G. Botton, T.M. Tritt, H. Kleinke, J. Alloys Compd. **504**, 314 (2010)
138. H. Xu, K.M. Kleinke, T. Holgate, H. Zhang, Z. Su, T.M. Tritt, H. Kleinke, J. Appl. Phys. **105**, 053703 (2009)
139. C. Candolfi, B. Lenoir, J. Leszczynski, A. Dauscher, E. Guilmeau, J. Appl. Phys. **105**, 083701 (2009)
140. S.R. Brown, S.M. Kauzlarich, F. Gascoin, G.J. Snyder, Chem. Mater. **18**, 1873 (2006)
141. C.A. Cox, E.S. Toberer, A.A. Levchenko, S.R. Brown, G.J. Snyder, A. Navrotsky, S.M. Kauzlarich, Chem. Mater. **21**, 1354 (2009)
142. C.A. Uvarov, J.F. Rauscher, S.M. Kauzlarich, Sci. Adv. Mater. **3**, 646 (2011)
143. C.A. Uvarov, F. Ortega-Alvarez, S.M. Kauzlarich, Inorg. Chem. **51**, 7617 (2012)
144. S.R. Brown, E.S. Toberer, T. Ikeda, C.A. Cox, F. Gascoin, S.M. Kauzlarich, G.J. Snyder, Chem. Mater. **20**, 3412 (2008)
145. T. Yi, M.N. Abdusalyamova, F. Makhmudovb, S.M. Kauzlarich, J. Mater. Chem. **22**, 14378 (2012)

146. E.S. Toberer, A. Zevalkink, N. Crisosto, G.J. Snyder, *Adv. Funct. Mater.* **20**, 4375 (2010)
147. A. Zevalkink, G.S. Pomrehn, S. Johnson, J. Swallow, Z.M. Gibbs, G.J. Snyder, *Chem. Mater.* **24**, 2091 (2012)
148. S.I. Johnson, A. Zevalkink, G.J. Snyder, *J. Mater. Chem. A* **1**, 4244 (2013)
149. A. Zevalkink, J. Swallow, G.J. Snyder, *Dalton Trans.* **42**, 9713 (2013)
150. A. Zevalkink, W.G. Zeier, G. Pomrehn, E. Schechtel, W. Tremel, G.J. Snyder, *Energy Environ. Sci.* **5**, 9121 (2012)
151. C.-J. Liu, Y.-L. Liu, H.-C. Lai, L.-R. Chen, Y.-Y. Zou, *J. Electron. Mater.* **42**, 1550 (2013)
152. K. Biswas, J. He, I.D. Blum, C.-I. Wu, T.P. Hogan, D.N. Seidman, V.P. Dravid, M.G. Kanatzidis, *Nature* **489**, 414 (2012)
153. M. Fujikane, K. Kurosaki, H. Muta, S. Yamanaka, *J. Alloys Compd.* **393**, 299 (2004)
154. F.D. Rosi, E.F. Hockings, N.E. Lindenblad, *RCA Rev.* **22**, 82 (1961)
155. R.W. Armstrong, J.W. Faust, W.A. Tiller, *J. Appl. Phys.* **31**, 1954 (1960)
156. Y. Noda, K. Mizuno, Y.S. Kang, M. Niino, I.A. Nishida, *J. Jpn Inst. Met.* **63**, 1448 (1999)
157. H. Ma, T. Su, P. Zhu, J. Guo, X. Ji, *J. Alloys Compd.* **454**, 415 (2008)
158. T. Su, X. Jia, H. Ma, F. Yu, Y. Tian, G. Zuo, Y. Zheng, Y. Jiang, D. Dong, L. Deng, B. Qin, S. Zheng, *J. Appl. Phys.* **105**, 073713 (2009)
159. J.D. Sugar, D.L. Medlina, *J. Alloys Compd.* **478**, 75 (2009)
160. S.N. Zhang, T.J. Zhu, S.H. Yang, C. Yu, X.B. Zhao, *J. Alloys Compd.* **499**, 215 (2010)
161. J. Xu, H. Li, B. Du, X. Tang, Q. Zhang, C. Uher, *J. Mater. Chem.* **20**, 6138 (2010)
162. V. Jovovic, J.P. Heremans, *J. Electron. Mater.* **38**, 1504 (2009)
163. B.L. Du, H. Li, X.F. Tang, *J. Alloys Compd.* **509**, 2039 (2011)
164. K.T. Wojciechowski, M. Schmidt, *Phys. Rev. B* **79**, 184202 (2009)
165. B. Du, H. Li, J. Xu, X. Tang, C. Uher, *Chem. Mater.* **22**, 5521 (2010)
166. B. Du, H. Li, J. Xu, X. Tang, C. Uher, *J. Solid State Chem.* **184**, 109 (2011)
167. D. Parker, D.J. Singh, *Phys. Rev. B* **85**, 125209 (2012)
168. A. Yusufu, K. Kurosaki, A. Kosuga, T. Sugahara, Y. Ohishi, H. Muta, S. Yamanaka, *Appl. Phys. Lett.* **99**, 061902 (2011)
169. Z. Ye, J.Y. Cho, M.M. Tessema, J.R. Salvador, R.A. Waldo, H. Wang, W. Cai, *J. Solid State Chem.* **201**, 262 (2013)
170. K. Kurosaki, H. Matsumoto, A. Charoenphakdee, S. Yamanaka, M. Ishimaru, Y. Hirotsu, *Appl. Phys. Lett.* **93**, 012101 (2008)
171. T. Plirdpring, K. Kurosaki, A. Kosuga, M. Ishimaru, A. Harnwungmoung, T. Sugahara, Y. Ohishi, H. Muta, S. Yamanaka, *Appl. Phys. Lett.* **98**, 172104 (2011)
172. J. Cui, Y. Gao, H. Zhou, Y. Li, Q. Meng, J. Yang, *Appl. Phys. Lett.* **101**, 081908 (2012)
173. F.D. Rosi, E.F. Hockings, N.E. Lindenblad, *Electrical Engineering* **79**, 450 (1960)
174. E.A. Skrabek, D.S. Trimmer, *Properties of the General TAGS System*, in *Handbook of Thermoelectrics* (CRC Press, 1994)
175. J.W. Sharp, in *Proceedings of 22nd ICT, La Grand Motte, France, August, 2003*, p. 267
176. E. Skrabek, D. Trimmer, US Patent No. 3 945 855, issued March 23 (1976)
177. G.C. Christakudis, S.K. Plachkova, L.E. Shelimova, E.S. Avilov, *Phys. Stat. Sol. A* **128**, 465 (1991)
178. S.K. Plachkova, I.A. Avramova, *Phys. Stat. Sol. A* **184**, 195 (2001)
179. S.H. Yang, T.J. Zhu, T. Sun, J. He, S.N. Zhang, X.B. Zhao, *Nanotechnology* **19**, 245707 (2008)
180. X.B. Zhao, S.H. Yang, Y.Q. Cao, J.L. Mi, Q. Zhang, T.J. Zhu, *J. Electron. Mater.* **38**, 1017 (2009)
181. S.N. Zhang, J. He, X.H. Ji, Z. Su, S.H. Yang, T.J. Zhu, X.B. Zhao, T.M. Tritt, *J. Electron. Mater.* **38**, 1142 (2009)
182. E.M. Levin, B.A. Cook, J.L. Harringa, S.L. Bud'ko, R. Venkatasubramanian, K. Schmidt-Rohr, *Adv. Funct. Mater.* **21**, 441 (2011)
183. E.M. Levin, S.L. Bud'ko, K. Schmidt-Rohr, *Adv. Funct. Mater.* **22**, 2766 (2012)
184. J. Davidow, Y. Gelbstein, *J. Electron. Mater.* **42**, 1542 (2013)
185. K.F. Hsu, S.L. Loo, F. Guo, W. Chen, J.S. Dyck, C. Uher, T. Hogan, E.K. Polychroniadis, M.G. Kanatzidis, *Science* **303**, 818 (2004)
186. E. Quarez, K.-F. Hsu, R. Pcionek, N. Frangis, E.K. Polychroniadis, M.G. Kanatzidis, *J. Am. Chem. Soc.* **127**, 917 (2005)
187. N. Chen, F. Gascoin, G.J. Snyder, E. Müller, G. Karpinski, C. Stiewe, *Appl. Phys. Lett.* **87**, 171903 (2005)
188. L. Wu, J.C. Zheng, J. Zhou, Q. Li, J. Yang, Y. Zhu, *J. Appl. Phys.* **105**, 094317 (2009)
189. A. Kosuga, M. Uno, K. Kurosaki, S. Yamanaka, *J. Alloys Compd.* **387**, 52 (2005)
190. A. Kosuga, M. Uno, K. Kurosaki, S. Yamanaka, *J. Alloys Compd.* **391**, 288 (2005)
191. H. Wang, J.F. Li, C.W. Nan, M. Zhou, W.S. Liu, B.P. Zhang, T. Kita, *Appl. Phys. Lett.* **88**, 092104 (2006)
192. M. Zhou, J.F. Li, T. Kita, *J. Am. Chem. Soc.* **130**, 4527 (2008)
193. Z.Y. Li, M. Zou, J.-F. Li, *J. Alloys Compd.* **549**, 319 (2013)
194. D. Bilc, S.D. Mahanti, E. Quarez, K.F. Hsu, R. Pcionek, M.G. Kanatzidis, *Phys. Rev. Lett.* **93**, 146403 (2004)
195. D.I. Bilc, S.D. Mahanti, M.G. Kanatzidis, *Phys. Rev. B* **74**, 125202 (2006)
196. H. Hazama, U. Mizutani, R. Asahi, *Phys. Rev. B* **73**, 115108 (2006)
197. S.V. Barabash, V. Ozolins, C. Wolverton, *Phys. Rev. Lett.* **101**, 155704 (2008)
198. X. Ke, C. Chen, J. Yang, L. Wu, J. Zhou, Q. Li, Y. Zhu, P.R.C. Kent, *Phys. Rev. Lett.* **103**, 145502 (2009)
199. M.K. Han, H. Kong, C. Uher, M.G. Kanatzidis, *Mater. Res. Soc. Symp. Proc.* **1044**, U03 (2008)
200. M.W. Oh, S.D. Park, B.S. Kim, B.K. Min, M.H. Kim, H.W. Lee, *Electron. Mater. Lett.* **8**, 659 (2012)
201. J. Androulakis, K.F. Hsu, R. Pcionek, H. Kong, C. Uher, J.J. D'Angelo, A. Downey, T. Hogan, M.G. Kanatzidis, *Adv. Mater.* **18**, 1170 (2006)
202. A. Kosuga, K. Kurosaki, H. Muta, S. Yamanaka, *J. Alloys Compd.* **416**, 218 (2006)
203. K. Ahn, M.G. Kanatzidis, *Mater. Res. Soc. Symp. Proc.* **1044**, U04 (2008)

204. P.F.P. Poudeu, J. D'Angelo, A.D. Downey, J.L. Short, T.P. Hogan, M.G. Kanatzidis, *Angew. Chem. Int. Ed. Engl.* **45**, 3835 (2006)
205. E.I. Rogacheva, O.N. Nashchekina, M.S. Dresselhaus, in *Proceedings of 22nd ICT, La Grand Motte, France, August, 2003*, p. 263
206. Q. Zhang, B. Liao, Y. Lan, K. Lukas, W. Liu, K. Esfarjani, C. Opeil, D. Broido, G. Chen, Z. Ren, *Proc. Natl. Acad. Sci. USA* **110**, 13261 (2013)
207. Y. Dong, A.S. Malik, F.J. DiSalvo, *J. Solid State Chem.* **183**, 1817 (2010)
208. Y. Gelbstein, B. Dado, O. Ben-Yehuda, Y. Sadia, Z. Dashevsky, M.P. Dariel, *Chem. Mater.* **22**, 1054 (2010)
209. Y. Rosenberg, Y. Gelbstein, M.P. Dariel, *J. Alloys Compd.* **526**, 31 (2012)
210. W. Pan, J. Gong, L. Zhang, L. Chen, *Mater. Sci. Forum* **423-4**, 367 (2003)
211. Y. Gelbstein, B. Dado, O. Ben-Yehuda, Y. Sadia, Z. Dashevsky, M.P. Dariel, *J. Electron. Mater.* **39**, 2049 (2010)
212. L. Zhang, W. Wang, B. Ren, J. Guo, *J. Electron. Mater.* **42**, 1303 (2013)
213. J.Q. Li, L.F. Li, S.H. Song, F.S. Liu, W.Q. Ao, *J. Alloys Compd.* **565**, 144 (2013)
214. T. Caillat, C.K. Huang, J.P. Fleurial, G.J. Snyder, A. Borshchevsky, in *Proceedings of 19th ICT, Cardiff, UK: IEEE Piscataway, NJ, 2000*, p. 151
215. J.F. Meng, N.V. Chandra Sekar, J.V. Badding, D.Y. Chung, M.G. Kanatzidis, *J. Appl. Phys.* **90**, 2836 (2001)
216. K. Kurosaki, K. Goto, H. Muta, S. Yamanaka, *J. Appl. Phys.* **102**, 023707 (2007)
217. M.W. Oh, D.M. Wee, S.D. Park, B.S. Kim, H.W. Lee, *Phys. Rev. B* **77**, 165119 (2008)
218. H. Matsumoto, K. Kurosaki, H. Muta, S. Yamanaka, *J. Appl. Phys.* **104**, 073705 (2008)
219. K. Kurosaki, H. Uneda, H. Muta, S. Yamanaka, *J. Alloys Compd.* **376**, 43 (2004)
220. J.W. Sharp, B.C. Sales, D. Mandrus, B.C. Chakoumakos, *Appl. Phys. Lett.* **74**, 3794 (1999)
221. B. Wolfing, C. Kloc, J. Teubner, E. Bucher, *Phys. Rev. Lett.* **86**, 4350 (2001)
222. K. Kurosaki, A. Kosuga, H. Muta, M. Uno, S. Yamanaka, *Appl. Phys. Lett.* **87**, 061919 (2005)
223. K. Kurosaki, S. Yamanaka, *Phys. Stat. Sol. A* **210**, 82 (2013)
224. D. Huo, G. Tang, C. Fu, L. Li, *J. Electron. Mater.* **40**, 1202 (2011)
225. L.R. Danielson, M.N. Alexander, C. Vining, R.A. Lockwood, C. Wood, in *Proceedings of 7th International Conference on Thermoelectrics Energy Conversion, University of Texas, Arlington, 1988*, p. 71
226. B.J. Beaudry, K.A. Gschneidner, *Rare Earth compounds* (1995), Chap. 19
227. A.F. May, J.P. Fleurial, G.J. Snyder, *Phys. Rev. B* **78**, 125205 (2008)
228. A. May, G.J. Snyder, J.P. Fleurial, *Lanthanum Telluride: Mechanochemical Synthesis of a Refractory Thermoelectric Material* (2008), p. 672
229. J.L. Cui, *J. Alloys Compd.* **415**, 216 (2006)
230. J. Cui, W. Xiu, H. Xue, *J. Appl. Phys.* **101**, 123713 (2007)
231. J.L. Cui, H.F. Xue, W.J. Xiu, L. Jiang, P.Z. Ying, *J. Solid State Chem.* **179**, 3751 (2006)
232. J.L. Cui, H.F. Xue, W.J. Xiu, *Intermetallics* **15**, 1466 (2007)
233. J.L. Cui, H. Fub, X.L. Liua, D.Y. Chenb, W. Yang, *Curr. Appl. Phys.* **9**, 1170 (2009)
234. J. Cui, X. Liu, W. Yang, D. Chen, H. Fu, P. Ying, *J. Appl. Phys.* **105**, 063703 (2009)
235. R.J. Mehta, Y. Zhang, H. Zhu, D.S. Parker, M. Belley, D.J. Singh, R. Ramprasad, T. Borca-Tasciuc, G. Ramanath, *Nano Lett.* **12**, 4523 (2012)
236. S. Wang, G.J. Snyder, T. Caillat, in *Proceedings of 21st ICT, Long Beach, California, USA, Aug. 25-29, 2002*, p. 170
237. V.L. Kuznetsov, L.A. Kuznetsova, D.M. Rowe, *J. Phys. D* **34**, 700 (2001)
238. Y.J. Shan, K. Sasaki, K. Sudo, H. Imoto, M. Itoh, *Jpn J. Appl. Phys.* **41**, L780 (2002)
239. P. Vaqueiro, G. Guélou, M. Stec, E. Guilmeau, A.V. Powell, *J. Mater. Chem. A* **1**, 520 (2013)
240. A. Maignan, E. Guilmeau, F. Gascoin, Y. Bréard, V. Hardy, *Sci. Technol. Adv. Mater.* **13**, 053003 (2012)
241. S. Hébert, W. Kobayashi, H. Muguerra, Y. Bréard, N. Raghavendra, F. Gascoin, E. Guilmeau, A. Maignan, *Phys. Stat. Sol. A* **210**, 69 (2013)
242. M. Telkes, Westinghouse research report, Pittsburg, USA, R-94264-B (1938)
243. M. Telkes, *J. Appl. Phys.* **18**, 1116 (1947)
244. I. Kudman, *Metall. Trans. A* **2**, 163 (1971)
245. I. Kudman, *J. Mater. Sci.* **7**, 1027 (1972)
246. J. Androulakis, D.-Y. Chung, X. Su, L. Zhang, C. Uher, T.C. Hasapis, E. Hatzikraniotis, K.M. Paraskevopoulos, M.G. Kanatzidis, *Phys. Rev. B* **84**, 155207 (2011)
247. J. Androulakis, Y. Lee, I. Todorov, D.-Y. Chung, M.G. Kanatzidis, *Phys. Rev. B* **83**, 195209 (2011)
248. B.A. Mansour, *Phys. Stat. Sol. A* **136**, 153 (1993)
249. Z.-H. Ge, B.-P. Zhang, Y.-X. Chen, Z.-X. Yu, Y. Liu, J.-F. Li, *Chem. Commun.* **47**, 12697 (2011)
250. D.R. Brown, T. Day, T. Caillat, G.J. Snyder, *J. Electron. Mater.* **42**, 2014 (2013)
251. H. Liu, X. Shi, F. Xu, L. Zhang, W. Zhang, L. Chen, Q. Li, C. Uher, T. Day, G.J. Snyder, *Nat. Mater.* **11**, 422 (2012)
252. H. Liu, X. Shi, M. Kirkham, H. Wang, Q. Li, C. Uher, W. Zhang, L. Chen, *Mater. Lett.* **93**, 121 (2013)
253. F. Gascoin, A. Maignan, *Chem. Mater.* **23**, 2510 (2011)
254. G.C. Tewari, T.S. Tripathi, A.K. Rastogi, *J. Electron. Mater.* **39**, 1133 (2010)
255. Y.-X. Chen, B.-P. Zhang, Z.-H. Ge, P.-P. Shang, *J. Solid State Chem.* **186**, 109 (2012)
256. S. Bhattacharya, R. Basu, R. Bhatt, A. Singh, D.K. Aswal, S.K. Gupta, *AIP Conf. Proc.* **1536**, 1233 (2013)
257. C.-G. Han, B.-P. Zhang, Z.-H. Ge, L.-J. Zhang, Y.-C. Liu, *J. Mater. Sci.* **48**, 4081 (2013)
258. S. Bhattacharya, R. Basu, R. Bhatt, S. Pitale, A. Singh, D.K. Aswal, S.K. Gupta, M. Navaneethan, Y. Hayakawa, *J. Mater. Chem. A* **1**, 11289 (2013)
259. S. Bhattacharya, R. Basu, R. Bhatt, A. Singh, S. Sen, D. Aswal, S.K. Gupta, *AIP Conf. Proc.* **1447**, 1021 (2012)
260. M. Ohta, S. Satoh, T. Kuzuya, S. Hirai, M. Kunii, A. Yamamoto, *Acta Mater.* **60**, 7232 (2012)
261. F. Gascoin, N. Raghavendra, E. Guilmeau, Y. Bréard, *J. Alloys Compd.* **521**, 121 (2012)
262. J. Zhang, X.Y. Qin, H.X. Xin, D. Li, C.J. Song, *J. Electron. Mater.* **40**, 980 (2011)

263. E. Guilmeau, Y. Bréard, A. Maignan, *Appl. Phys. Lett.* **99**, 052107 (2011)
264. R. Bhatt, S. Bhattacharya, R. Basu, A. Singh, D.K. Aswal, S.K. Gupta, *AIP Conf. Proc.* **1512**, 1004 (2013)
265. R. Bhatt, R. Basu, S. Bhattacharya, A. Singh, D.K. Aswal, S.K. Gupta, G.S. Okram, V. Ganesan, D. Venkateshwarlu, C. Surgers, M. Navaneethan, Y. Hayakawa, *Appl. Phys. A* **111**, 465 (2013)
266. T.C. Holgate, S. Zhu, M. Zhou, S. Bangarigadu-Sanasy, H. Kleinke, J. He, T.M. Tritt, *J. Solid State Chem.* **197**, 273 (2013)
267. T.C. Holgate, Y. Liu, D. Hitchcock, T.M. Tritt, J. He, *J. Electron. Mater.* **42**, 1751 (2013)
268. H. Imai, Y. Shimakawa, T. Manako, Y. Kubo, *Jpn Soc. Appl. Phys. Ext. Abst. (49th Spring Meeting 2002)* **29a**, S-1 (2002)
269. C. Wan, Y. Wang, N. Wang, W. Norimitsu, M. Kusunoki, K. Koumoto, *J. Electron. Mater.* **40**, 1271 (2011)
270. T. Aoki, C. Wan, H. Ishiguro, H. Morimitsu, K. Koumoto, *J. Ceram. Soc. Jpn* **119**, 382 (2011)
271. C. Wan, Y. Wang, N. Wang, K. Koumoto, *Mater. Chem. Phys.* **3**, 2606 (2010)
272. Y.E. Putri, C. Wan, Y. Wang, W. Norimatsu, M. Kusunokic, K. Koumoto, *Scripta Mater.* **66**, 895 (2012)
273. Y.E. Putri, C. Wan, R. Zhang, T. Mori, K. Koumoto, *J. Adv. Ceram.* **2**, 42 (2013)
274. Y. Miyazaki, H. Ogawa, T. Nakajo, Y. Kikuchii, K. Hayashi, *J. Electron. Mater.* **42**, 1335 (2013)
275. F.M. Ryan, I.N. Greenberg, F.L. Carter, R.C. Miller, *J. Appl. Phys.* **33**, 864 (1962)
276. T. Takeshita, K.A. Gschneidner, B.J. Beaudry, *J. Appl. Phys.* **57**, 4633 (1985)
277. C. Wood, A. Lockwood, J. Parker, A. Zoltan, D. Zoltan, L.R. Danielson, V. Ragg, *J. Appl. Phys.* **58**, 1542 (1985)
278. J.F. Nakahara, T. Takeshita, M.J. Tschetter, B.J. Beaudry, K.A. Gschneidner, in *Proceedings of 1st European Conference on Thermoelectrics, Cardiff, Wales, 1988*, edited by D.M. Rowe, p. 161
279. M. Ohta, H. Yuan, S. Hirai, Y. Yajima, T. Nishimura, K. Shimakage, *J. Alloys Compd.* **451**, 627 (2008)
280. M. Ohta, T. Kuzuya, H. Sasaki, T. Kawasaki, S. Hirai, *J. Alloy Phase Diagrams* **484**, 268 (2009)
281. S. Katsuyama, Y. Tanaka, H. Hashimoto, K. Majima, H. Nagai, *J. Appl. Phys.* **82**, 5513 (1997)
282. M.G. Kanatzidis, T.J. McCarthy, T.A. Tanzer, L.-H. Chen, L. Iordanidis, *Chem. Mater.* **8**, 1465 (1996)
283. D.-Y. Chung, K.-S. Choi, L. Iordanidis, J.L. Schindler, P.W. Brazis, C.R. Kannewurf, B. Chen, S. Hu, C. Uher, M.G. Kanatzidis, *Chem. Mater.* **9**, 3060 (1997)
284. T. Kyratsi, M. Ioannou, *J. Electron. Mater.* **42**, 1604 (2013)
285. D. Liang, R. Ma, S. Jiao, G. Pang, S. Feng, *Nanoscale* **4**, 6265 (2012)
286. N. Tsujii, *J. Electron. Mater.* **42**, 1974 (2013)
287. N. Tsujii, T. Mori, *Appl. Phys. Express* **6**, 043001 (2013)
288. J. Li, Q. Tan, J.-F. Li, *J. Alloys Compd.* **551**, 143 (2013)
289. J.Y. Cho, X. Shi, J.R. Salvador, J. Yang, H. Wang, *J. Appl. Phys.* **108**, 073713 (2010)
290. M. Ibáñez, D. Cadavid, U. Anselmi-Tamburini, R. Zamani, S. Gorsse, W. Li, A.M. López, J.R. Morante, J. Arbiol, A. Cabot, *J. Mater. Chem. A* **1**, 1421 (2013)
291. M. Ibáñez, R. Zamani, W. Li, D. Cadavid, S. Gorsse, N.A. Katcho, A. Shavel, A.M. López, J.R. Morante, J. Arbiol, A. Cabot, *Chem. Mater.* **24**, 4615 (2012)
292. J.Y. Cho, X. Shi, J.R. Salvador, G.P. Meisner, J. Yang, H. Wang, A.A. Wereszczak, X. Zhou, C. Uher, *Phys. Rev. B* **84**, 085207 (2011)
293. L. Xi, Y.B. Zhang, X.Y. Shi, J. Yang, X. Shi, L.D. Chen, W. Zhang, J. Yang, D.J. Singh, *Phys. Rev. B* **86**, 155201 (2012)
294. X. Shi, L. Xi, J. Fan, W. Zhang, L. Chen, *Chem. Mater.* **22**, 6029 (2010)
295. Y. Zhang, E.J. Skoug, J. Cain, V. Ozolins, D.T. Morelli, C. Wolverton, *Phys. Rev. B* **85**, 054306 (2012)
296. M.-L. Liu, I.-W. Chen, F.-Q. Huang, L.-D. Chen, *Adv. Mater.* **21**, 3808 (2009)
297. M.L. Liu, F.G. Huang, L.D. Chen, I.W. Chen, *Appl. Phys. Lett.* **94**, 202103 (2009)
298. X.Y. Shi, F.Q. Huang, M.L. Liu, L.D. Chen, *Appl. Phys. Lett.* **94**, 122103 (2009)
299. M. Ibáñez, D. Cadavid, R. Zamani, N. García-Castelló, V. Izquierdo-Roca, W. Li, A. Fairbrother, J.D. Prades, A. Shavel, J. Arbiol, A. Pérez-Rodríguez, J.R. Morante, A. Cabot, *Chem. Mater.* **24**, 562 (2012)
300. C. Yang, F. Huang, L. Wu, K. Xu, *J. Phys. D* **44**, 295404 (2011)
301. X.Y. Li, D. Li, H.X. Xin, J. Zhang, C.J. Song, X.Y. Qin, *J. Alloys Compd.* **561**, 105 (2013)
302. E.J. Skoug, J.D. Cain, D.T. Morelli, *Appl. Phys. Lett.* **98**, 261911 (2011)
303. K. Suekuni, K. Tsuruta, T. Ariga, M. Koyano, *Appl. Phys. Express* **5**, 051201 (2012)
304. X. Lu, D.T. Morelli, Y. Xia, F. Zhou, V. Ozolins, H. Chi, X. Zhou, C. Uher, *Adv. Energy Mater.* **3**, 342 (2013)
305. K. Suekuni, K. Tsuruta, M. Kunii, H. Nishiate, E. Nishibori, S. Maki, M. Ohta, A. Yamamoto, M. Koyano, *J. Appl. Phys.* **113**, 043712 (2013)
306. X. Lu, D.T. Morelli, *Phys. Chem. Chem. Phys.* **15**, 5762 (2013)
307. R. Carlini, C. Artini, G. Borzone, R. Masini, G. Zanichchi, G.A. Costa, *J. Therm. Anal. Calorim.* **103**, 23 (2011)
308. D. Parker, A.F. May, H. Wang, M.A. McGuire, B.C. Sales, D.J. Singh, *Phys. Rev. B* **87**, 045205 (2013)
309. D. Li, X.Y. Qin, *J. Appl. Phys.* **100**, 023713 (2006)
310. C. Xiao, J. Xu, B. Cao, K. Li, M. Kong, Y. Xie, *J. Am. Chem. Soc.* **134**, 7971 (2012)
311. C. Xiao, X. Qin, J. Zhang, R. An, J. Xu, K. Li, B. Cao, J. Yang, B. Ye, Y. Xie, *J. Am. Chem. Soc.* **134**, 18460 (2012)
312. L. Pan, D. Bérardan, N. Dragoe, *J. Am. Chem. Soc.* **135**, 4914 (2013)
313. H. Nishiate, M. Ohta, A. Yamamoto, H. Obara, C.-H. Lee, K. Ueno, *Mater. Trans. JIM* **52**, 1535 (2011)
314. M. Ohta, H. Obara, A. Yamamoto, *Mater. Trans.* **50**, 2129 (2009)
315. T. Caillat, J.P. Fleurial, G.J. Snyder, *Solid State Sci.* **1**, 535 (1999)
316. Y. Ohta, J. Rousseau, J. Tobola, P. Pêcheur, H. Scherrer, I. Iwanaga, A. Kasama, Y. Matsumura, in *Proceedings of 22nd ICT, La Grand Motte, France, August, 2003*, p. 255
317. A.M. Schmidt, M.A. McGuire, F. Gascoin, G.J. Snyder, F.J. DiSalvo, *J. Alloys Compd.* **431**, 262 (2007)
318. T. Zhou, B. Lenoir, M. Colin, A. Dauscher, R.A.R.A. Orabi, P. Gougeon, M. Potel, E. Guilmeau, *Appl. Phys. Lett.* **98**, 162106 (2011)
319. J.-S. Rhyee, K.H. Lee, S.M. Lee, E. Cho, S. II Kim, E. Lee, Y.S. Kwon, J.H. Shim, G. Kotliar, *Nature* **459**, 965 (2009)

320. J.-S. Rhyee, K. Ahn, K.H. Lee, H.S. Ji, J.-H. Shim, *Adv. Mater.* **23**, 2191 (2011)
321. K. Ahn, E. Cho, J.-S. Rhyee, S. II Kim, S. Hwang, H.-S. Kim, S.M. Lee, K.H. Lee, *J. Mater. Chem.* **22**, 5730 (2012)
322. J.-S. Rhyee, E. Cho, K.H. Lee, S.M. Lee, S. II Kim, H.-S. Kim, Y.S. Kwon, S.J. Kim, *Appl. Phys. Lett.* **95**, 212106 (2009)
323. X. Shi, J.Y. Cho, J.R. Salvador, J. Yang, H. Wang, *Appl. Phys. Lett.* **96**, 162108 (2010)
324. J.-S. Rhyee, D. Choi, *J. Appl. Phys.* **110**, 083706 (2011)
325. K. Ahn, E. Cho, J.-S. Rhyee, S. II Kim, S.M. Lee, K.H. Lee, *Appl. Phys. Lett.* **99**, 102110 (2011)
326. J. Cui, X. Liu, X. Zhang, Y. Li, Y. Deng, *J. Appl. Phys.* **110**, 023708 (2011)
327. Y. Zhai, Q. Zhang, J. Jiang, T. Zhang, Y. Xiao, S. Yang, G. Xu, *J. Mater. Chem. A* **1**, 8844 (2013)
328. J.L. Cui, Y.Y. Li, Y. Deng, Q.S. Meng, Y.L. Gao, H. Zhou, Y.P. Li, *Intermetallics* **31**, 217 (2012)
329. H. Takahashi, N. Raghavendra, F. Gascoin, D. Pelloquin, S. Hébert, E. Guilmeau, *Chem. Mater.* **25**, 1809 (2013)
330. L.D. Zhao, D. Bérardan, Y.L. Pei, C. Byl, L. Pinsard-Gaudart, N. Dragoe, *Appl. Phys. Lett.* **97**, 092118 (2010)
331. F. Li, J.-F. Li, L.-D. Zhao, K. Xiang, Y. Liu, B.-P. Zhang, Y.-H. Lin, C.-W. Nan, H.-M. Zhu, *Energy Environ. Sci.* **5**, 7188 (2012)
332. J. Li, J.H. Sui, Y.L. Pei, C. Barreateau, D. Berardan, N. Dragoe, J.Q. He, L.D. Zhao, *Energy Environ. Sci.* **5**, 8543 (2012)
333. C. Barreateau, D. Bérardan, E. Amzallag, L.D. Zhao, N. Dragoe, *Chem. Mater.* **24**, 3168 (2012)
334. J. Li, J. Sui, C. Barreateau, D. Bérardan, N. Dragoe, W. Cai, Y. Pei, L.-D. Zhao, *J. Alloys Compd.* **551**, 649 (2013)
335. Y.-L. Pei, J. He, J.-F. Li, F. Li, Q. Liu, W. Pan, C. Barreateau, D. Berardan, N. Dragoe, L.-D. Zhao, in *Proceedings of NPG Asia Materials, 2013*, p. e47
336. J.-L. Lan, B. Zhan, Y.-C. Liu, B. Zheng, Y. Liu, Y.-H. Lin, C.-W. Nan, *Appl. Phys. Lett.* **102**, 123905 (2013)
337. C. Wood, *Rep. Prog. Phys.* **51**, 459 (1988)
338. M. Takeda, T. Fukuda, T. Miura, in *Proceedings of 21st International ICT, Long Beach, California, USA, Aug. 25–29, 2002*, p. 173
339. T. Mori, T. Nishimura, *J. Sol. Stat. Chem.* **179**, 2908 (2006)
340. T. Mori, K. Nishimura, in *Proceedings of ICT06, Vienna, Austria, 2006*, pp. 164–167
341. T. Mori, *J. Appl. Phys.* **97**, 093703 (2006)
342. L.D. Chen, T. Goto, J.H. Li, T. Hirai, *Mater. Trans. JIM* **37**, 1182 (1996)
343. J. Li, T. Goto, T. Hirai, *Mater. Trans. JIM* **40**, 314 (1999)
344. S. Ghamaty, N.B. Elsne, *Mat. Res. Soc. Symp. Proc.* **793**, S8.13.1 (2003)
345. V. Jovanovic, S. Ghamaty, D. Krommenhoek, J.C. Bass, in *Proceedings of IPACK 2007, Vancouver, British Columbia, Canada, 8–12 July, 2007*, pp. 1–7
346. Y. Amagai, A. Yamamoto, T. Iida, Y. Takanashi, *J. Appl. Phys.* **96**, 5644 (2004)
347. C.S. Lue, W.J. Lai, Y.K. Kuo, *J. Alloys Compd.* **392**, 72 (2005)
348. Y. Hadano, S. Narazu, M.A. Avila, T. Onimaru, T. Takabatake, *J. Phys. Soc. Jpn* **78**, 013702 (2009)
349. Y. Amagai, A. Yamamoto, T. Iida, Y. Takanashi, in *Proceedings of 23rd ICT, Adelaide, Australia 25–29 July, 2004*, p. 148
350. Y. Takagiwa, J.T. Okada, K. Kimura, *J. Alloys Compd.* **507**, 364 (2010)
351. Y. Takagiwa, K. Kitahara, K. Kimura, *J. Appl. Phys.* **113**, 023713 (2013)
352. C.-E. Kim, K. Kurosaki, H. Muta, Y. Ohishi, S. Yamanaka, *J. Appl. Phys.* **111**, 043704 (2012)
353. T. Nakayama, K. Kurosaki, M. Shuto, C.-E. Kim, Y. Ohishi, H. Muta, S. Yamanaka, *J. Electron. Mater.* **42**, 1719 (2013)
354. D. Stark, G.J. Snyder, in *Proceedings of 21st ICT, Long Beach, California, USA, Aug. 25–29, 2002*, p. 181
355. H.F. Wang, K.F. Cai, H. Li, L. Wang, C.W. Zhou, *J. Alloys Compd.* **477**, 519 (2009)
356. C. Yu, T.J. Zhu, S.N. Zhang, X.B. Zhao, J. He, Z. Su, T.M. Tritt, *J. Appl. Phys.* **104**, 013705 (2008)
357. Q.G. Cao, H. Zhang, M.B. Tang, H.H. Chen, X.X. Yang, Y.N. Grin, J.T. Zhao, *J. Appl. Phys.* **107**, 053714 (2010)
358. X.-J. Wang, M.-B. Tang, H.-H. Chen, X.-X. Yang, J.-T. Zhao, U. Burkhardt, Y. Grin, *Appl. Phys. Lett.* **94**, 092106 (2009)
359. A.F. May, M.A. McGuire, D.J. Singh, J. Ma, O. Delaire, A. Huq, W. Cai, H. Wang, *Phys. Rev. B* **85**, 035202 (2012)
360. J. Chen, D. Wang, Z. Shuai, *J. Chem. Theor. Comput.* **8**, 3338 (2012)
361. Y. Nogami, H. Kaneko, T. Ishiguro, A. Takahashi, J. Tsukamoto, N. Hosoi, *Sol. Stat. Commun.* **76**, 583 (1990)
362. O. Bubnova, Z.U. Khan, A. Malti, S. Braun, M. Fahlman, M. Berggren, X. Crispin, *Nat. Mater.* **10**, 429 (2011)
363. Y. Sun, P. Sheng, C. Di, F. Jiao, W. Xu, D. Qiu, D. Zhu, *Adv. Mater.* **24**, 932 (2012)
364. G.-H. Kim, L.Y. Shao, K.Y. Zhang, K.Y.P. Pipe, *Nat. Mater.* **12**, 719 (2013)
365. T.O. Poehler, H.E. Katz, *Energy Environ. Sci.* **5**, 8110 (2012)
366. J. Yang, H.-L. Yip, A.K.-Y. Jen, *Adv. Energy Mater.* **3**, 549 (2013)
367. M. He, F. Qiu, Z. Lin, *Energy Environ. Sci.* **6**, 1352 (2013)
368. F. Cyrot-Lackmann, *Mater. Sci. Eng. A* **294**, 611 (2000)
369. K. Kirihara, K. Kimura, *J. Appl. Phys.* **92**, 979 (2002)
370. Y. Takagiwa, T. Kamimura, S. Hosoi, J.T. Okada, K. Kimura, *J. Appl. Phys.* **104**, 073721 (2008)
371. A.P. Gonçalves, E.B. Lopes, C. Godart, E. Alleno, O. Rouleau, Portuguese patent **103351** (2006)
372. A.P. Gonçalves, E.B. Lopes, O. Rouleau, C. Godart, *J. Mater. Chem.* **20**, 1516 (2010)
373. A.P. Gonçalves, G. Delaizir, E.B. Lopes, L.M. Ferreira, O. Rouleau, C. Godart, *J. Electron. Mater.* **40**, 1015 (2011)
374. J.B. Vaney, G. Delaizir, E. Alleno, O. Rouleau, A. Piarristeguy, J. Monnier, C. Godart, M. Ribes, R. Escalier, A. Pradel, A.P. Gonçalves, E.B. Lopes, G. Cuello, P. Ziolkowski, E. Muller, C. Candolfi, A. Dauscher, B. Lenoir, *J. Mater. Chem.* **1**, 8190 (2013)
375. R.J. Gambino, W.D. Grobman, A.M. Toxen, *Appl. Phys. Lett.* **22**, 506 (1973)
376. D.M. Rowe, G. Min, V.L. Kuznetsov, *Philos. Mag. Lett.* **77**, 105 (1998)
377. B. Buschinger, C. Geibel, F. Steglich, D. Mandrus, D. Young, J.L. Sarrao, Z. Fisk, *Physica B* **230**, 784 (1997)
378. A. Bentien, G.K.H. Madsen, S. Johnsen, B.B. Iversen, *Phys. Rev. B* **74**, 205105 (2006)

379. N. Oeschler, S. Hartmann, U. Köhler, M. Deppe, P. Sun, F. Steglich, in *Properties and applications of thermoelectric materials*, NATO Science for Peace and Security Series B – Physics and Biophysics (Springer, 2009), pp. 81–90
380. R. Lackner, E. Bauer, P. Rogl, *Physica B* **378**, 835 (2006)
381. S. Katsuyama, M. Suzuki, T. Tanaka, *J. Alloys Compd.* **513**, 189 (2012)
382. S.R. Boona, D.T. Morelli, *J. Appl. Phys.* **112**, 063709 (2012)
383. T. He, T.G. Calvarese, J.-Z. Chen, H.D. Rosenfeld, R.J. Small, J.J. Krajewski, M.A. Subramanian, in *24th International Conference on thermoelectrics, 2005*, p. 434
384. S.R. Boona, D.T. Morelli, *J. Electron. Mater.* **41**, 1199 (2012)
385. R. Boona, D.T. Morelli, *Appl. Phys. Lett.* **101**, 101909 (2012)
386. S.R. Boona, D.T. Morelli, *J. Electron. Mater.* **42**, 1592 (2013)
387. G.J. Lehr, D.T. Morelli, *Intermetallics* **32**, 225 (2013)
388. G.J. Lehr, D.T. Morelli, *J. Electron. Mater.* **42**, 1697 (2013)
389. P. Sun, T. Ikeno, T. Mizushima, Y. Isikawa, *Phys. Rev. B* **80**, 193105 (2009)
390. C.D.W. Jones, K.A. Regan, F.J. DiSalvo, *Phys. Rev. B* **58**, 16057 (1998)
391. A. Bentien, S. Johnsen, G.K.H. Madsen, B.B. Iversen, F. Steglich, *Europhys. Lett.* **80**, 17008 (2009)
392. P. Sun, N. Oeschler, S. Johnsen, B.B. Iversen, F. Steglich, *Dalton Trans.* **39**, 1012 (2010)
393. H. Zhao, M. Pokharel, S. Chen, B. Liao, K. Lukas, C. Opeil, G. Chen, Z. Ren, *Nanotechnology* **23**, 505402 (2012)
394. K. Wang, R. Hu, J. Warren, C. Petrovic, *J. Appl. Phys.* **112**, 013703 (2012)
395. H. Zhao, M. Pokharel, G. Zhu, S. Chen, K. Lukas, Q. Jie, C. Opeil, G. Chen, Z. Ren, *Appl. Phys. Lett.* **99**, 163101 (2011)
396. A. Datta, G.S. Nolas, *Eur. J. Inorg. Chem.* **1**, 55 (2012)
397. M. Pokharel, H. Zhao, K. Lukas, Z. Ren, C. Opeil, B. Mihaila, in *MRS Communications, 2013*, pp. 1–6
398. P. Sun, M. Søndergaard, Y. Sun, S. Johnsen, B.B. Iversen, F. Steglich, *Appl. Phys. Lett.* **98**, 072105 (2011)
399. M. Tomczak, K. Haule, T. Miyake, A. Georges, G. Kotliar, *Phys. Rev. B* **82**, 085104 (2010)
400. H. Takahashi, R. Okazaki, Y. Yasui, I. Terasaki, *Phys. Rev. B* **84**, 205215 (2011)
401. B.C. Sales, O. Delaire, M.A. McGuire, A.F. May, *Phys. Rev. B* **83**, 125209 (2011)
402. D.Y. Chung, T.P. Hogan, P. Brazis, M. Rocci-Lane, C.R. Kannewurf, M. Bastea, C. Uher, M.G. Kanatzidis, *Science* **287**, 1024 (2000)
403. P. Larson, S.D. Mahanti, D.Y. Chung, M.G. Kanatzidis, *Phys. Rev. B* **65**, 045205 (2002)
404. D.Y. Chung, C. Uher, M.G. Kanatzidis, *Chem. Mater.* **24**, 1854 (2012)
405. T. Okuda, W. Hirata, A. Takemori, S. Suzuki, S. Saijo, S. Miyasaka, S. Tajima, *J. Phys. Soc. Jpn* **80**, 044704 (2011)
406. J. Fukuyado, K. Narikiyo, M. Akaki, H. Kuwahara, T. Okuda, *Phys. Rev. B* **85**, 075112 (2012)
407. T. Nagase, I. Yamauchi, I. Ohnaka, *J. Alloys Compd.* **312**, 295 (2000)
408. K. Yanagimoto, K. Majima, S. Sunada, T. Sawada, *J. Alloys Compd.* **377**, 174 (2004)
409. Y. Zhao, J.S. Dyck, C. Burda, *J. Mater. Chem.* **21**, 17049 (2011)
410. J.Y. Yang, T. Aizawa, A. Yamamoto, T. Ohta, *J. Alloys Compd.* **312**, 326 (2000)
411. L. Xue-Dong, Y.-H. Park, *Mater. Transact. JIM* **43**, 30 (2002)
412. T. Tokiai, T. Uesugi, Y. Etoh, S. Tamura, Y. Yoneyama, K. Koumoto, *J. Ceram. Soc. Jpn* **104**, 837 (1996)
413. A. Sugiyama, K. Kobayashi, K. Ozaki, T. Nishio, A. Matsumoto, *J. Jpn Inst. Met.* **62**, 1082 (1998)
414. X.A. Fan, J.Y. Yang, W. Zhu, S.Q. Bao, X.K. Duan, C.J. Xiao, K. Li, *J. Alloys Compd.* **461**, 9 (2008)
415. M.K. Keshavarz, D. Vasilevskiy, R.A. Masut, S. Turenne, *J. Electron. Mater.* **42**, 1429 (2013)
416. D.L. Medlin, G.J. Snyder, *Curr. Opin. Colloid Interface Sci.* **14**, 226 (2009)
417. A.P. Gonçalves, E.B. Lopes, E. Alleno, C. Godart, in *Proceedings of 6th European Conference on Thermoelectrics ECT 2008, Paris July 2–4, 2008*, pp. P2–26
418. S.N. Zhang, J. He, T.J. Zhu, X.B. Zhao, T.M. Tritt, *J. Non-Cryst. Solids* **355**, 79 (2009)
419. F. Yan, T.J. Zhu, X.B. Zhao, S.R. Dong, *Appl. Phys. A: Mater. Sci. Proc.* **88**, 425 (2007)
420. X. Tang, W. Xie, H. Li, W. Zhao, Q. Zhang, M. Niino, *Appl. Phys. Lett.* **90**, 012102 (2007)
421. J.L. Harringa, B.A. Cook, *Mater. Sci. Eng. B* **60**, 137 (1999)
422. T. Hattori, Y. Iwadate, T. Sato, *J. Am. Ceram. Soc.* **73**, 140 (2005)
423. J.P. Heremans, V. Jovovic, E.S. Toberer, A. Saramat, K. Kurosaki, A. Charoenphakdee, S. Yamanaka, G.J. Snyder, *Science* **321**, 554 (2008)
424. B. Yu, Q. Zhang, H. Wang, X. Wang, H.F. Wang, D. Wang, H. Wang, G.J. Snyder, G. Chen, Z.F. Ren, *J. Appl. Phys.* **108**, 016104 (2010)
425. B. Poudel, Q. Hao, Y. Ma, Y. Lan, A. Minnich, B. Yu, X. Yan, D. Wang, A. Muto, D. Vashace, X. Chen, J. Liu, M.S. Dresselhaus, G. Chen, Z. Ren, *Science* **320**, 634 (2008)
426. Y. Ma, Q. Hao, B. Poudel, Y. Lan, B. Yu, D. Wang, G. Chen, Z. Ren, *Nano Lett.* **8**, 2580 (2008)
427. K.X. Zhang, X.Y. Qin, H.X. Xin, H.J. Li, J. Zhang, *J. Alloys Compd.* **484**, 498 (2009)
428. A.Y. Samunin, V.K. Zaitsev, P.P. Konstantinov, M.I. Fedorov, G.N. Isachenko, A.T. Burkov, S.V. Novikov, E.A. Gurieva, *J. Electron. Mater.* **42**, 1676 (2013)
429. C. Drasar, V. Kucek, L. Benes, P. Lostak, M. Vlcek, *J. Solid State Chem.* **193**, 42 (2012)
430. S. Bux, R. Blair, P. Gogna, H. Lee, G. Chen, M.S. Dresselhaus, R. Kaner, J.P. Fleurial, *Adv. Funct. Mater.* **19**, 2445 (2009)
431. S. Bux, J.P. Fleurial, R. Blair, P. Gogna, T. Caillat, R. Kaner, in *Proceedings of Mater. Res. Soc. Symp. Proc., 2009*, pp. N02–04
432. T.P. Hogan, A. Downey, J. Short, J. D’Angelo, C.-I. Wu, E. Quarez, J. Androulakis, P.F.P. Poudeu, J.R. Sootsman, D.Y. Chung, M.G. Kanatzidis, S.D. Mahanti, E.J. Timm, H. Schock, F. Ren, J. Johnson, E.D. Case, *J. Electron. Mater.* **36**, 704 (2007)

433. D.M. Hulbert, A. Anders, D.V. Dudina, J. Andersson, D. Jiang, C. Unuvar, U. Anselmi-Tamburini, E.J. Lavernia, A.K. Mukherjee, *J. Appl. Phys.* **104**, 033305 (2008)
434. R. Orrù, R. Licheri, A.M. Locci, A. Cincotti, G. Cao, *Mater. Sci. Eng. R* **63**, 127 (2009)
435. P.R. Sahm, H. Gnau, *Zeitschrift für Metallkunde* **59**, 137 (1968)
436. J.L. Mi, T.J. Zhu, X.B. Zhao, J. Ma, *J. Appl. Phys.* **101**, 054314 (2007)
437. K.F. Cai, C. Yan, Z.M. He, J.L. Cui, C. Stiewe, E. Müller, H. Li, *J. Alloys Compd.* **469**, 499 (2009)
438. K.F. Cai, X.R. He, M. Avdeev, D.H. Yu, J.L. Cui, H. Li, *J. Solid State Chem.* **181**, 1434 (2008)
439. G. Joshi, H. Lee, Y.C. Lan, X.W. Wang, G.H. Zhu, D.Z. Wang, R.W. Gould, D.C. Cuff, M.Y. Tang, M.S. Dresselhaus, G. Chen, Z.F. Ren, *Nano Lett.* **8**, 4670 (2008)
440. M. Mikami, K. Kobayashi, *J. Alloys Compd.* **466**, 530 (2008)
441. M. Mikami, A. Matsumoto, K. Kobayashi, *J. Alloys Compd.* **461**, 423 (2008)
442. J. Martin, G.S. Nolas, W. Zhang, L. Chen, *Appl. Phys. Lett.* **90**, 222112 (2007)
443. J. Martin, S. Stefanoski, L. Wang, L. Chen, G.S. Nolas, in *Proceedings of Mater. Res. Soc. Symp. Proc., 2008*, pp. U01–05
444. L.D. Zhao, B.P. Zhang, W.S. Liu, J.F. Li, *J. Appl. Phys.* **105**, 023704 (2009)
445. X.X. Li, J.Q. Li, F.S. Liu, W.Q. Ao, H.T. Li, L.C. Pan, *J. Alloys Compd.* **547**, 86 (2013)
446. J.Q. Li, X.X. Li, F.S. Liu, W.Q. Ao, H.T. Li, *J. Electron. Mater.* **42**, 366 (2013)
447. M. Søndergaard, M. Christensen, K.A. Borup, H. Yin, B.B. Iversen, *J. Electron. Mater.* **42**, 1417 (2013)
448. C. Chubilleau, B. Lenoir, P. Masschelein, A. Dauscher, C. Candolfi, E. Guilmeau, C. Godart, *J. Alloys Compd.* **554**, 340 (2013)
449. E. Alleno, M. Gaborit, V. Ohorodniichuk, B. Lenoir, O. Rouleau, *J. Electron. Mater.* **42**, 1835 (2013)
450. C. Chubilleau, B. Lenoir, A. Dauscher, C. Godart, *Intermetallics* **22**, 47 (2012)
451. J.S. Lin, Y. Miyamoto, *Mater. Res. Soc.* **15**, 647 (2000)
452. S.B. Cronin, Y.H. Lin, O. Rabin, M.R. Black, G. Dresselhaus, M.S. Dresselhaus, in *Proceedings of ICT'02, 21st ICT, Long Beach, CA, USA, 2001*, pp. 243–248
453. S.B. Cronin, Ph.D. Thesis, Massachusetts Institute of Technology, 2002
454. D. Zhao, L. Wang, Y. Cai, W. Jiang, L. Chen, *Mater. Sci. Forum* **610**, 389 (2009)
455. D. Zhao, M. Zuo, H. Geng, *Intermetallics* **31**, 321 (2012)
456. D. Zhao, X. Li, L. He, W. Jiang, L. Chen, *J. Alloys Compd.* **477**, 425 (2009)
457. K. Biswas, S. Muir, M.A. Subramanian, *Mater. Res. Bull.* **46**, 2288 (2011)
458. J. Arreguin-Zavala, D. Vasilevskiy, S. Turenne, R.A. Masut, *J. Electron. Mater.* **42**, 1992 (2013)
459. G. Delaizir, G. Bernard-Granger, J. Monnier, R. Grodzki, O. Kim-Hak, P.D. Szkutnik, M. Soulier, S. Saunier, D. Goeuriot, O. Rouleau, J. Simon, C. Godart, C. Navone, *Mater. Res. Bull.* **47**, 1954 (2012)